



Investigation of the nonlinear slamming-induced whipping response of ships using a fully-coupled hydroelastoplastic method

George Jagite, Quentin Derbanne, Sime Malenica, Fabien Bigot, Herve Le Sourn, Patrice Cartraud

► To cite this version:

George Jagite, Quentin Derbanne, Sime Malenica, Fabien Bigot, Herve Le Sourn, et al.. Investigation of the nonlinear slamming-induced whipping response of ships using a fully-coupled hydroelastoplastic method. Ocean Engineering, 2021, 238, pp.109751. 10.1016/j.oceaneng.2021.109751 . hal-04667468

HAL Id: hal-04667468

<https://hal.science/hal-04667468v1>

Submitted on 19 Nov 2024

HAL is a multi-disciplinary open access archive for the deposit and dissemination of scientific research documents, whether they are published or not. The documents may come from teaching and research institutions in France or abroad, or from public or private research centers.

L'archive ouverte pluridisciplinaire **HAL**, est destinée au dépôt et à la diffusion de documents scientifiques de niveau recherche, publiés ou non, émanant des établissements d'enseignement et de recherche français ou étrangers, des laboratoires publics ou privés.



Distributed under a Creative Commons Attribution - NonCommercial 4.0 International License

Investigation of the nonlinear slamming-induced whipping response of ships using a fully-coupled hydroelastoplastic method

George Jagite ^{a,*}, Quentin Derbanne ^b, Sime Malenica ^b, Fabien Bigot ^b, Herve Le Sourne ^c, Patrice Cartraud ^c

^a Bureau Veritas, Research Department, Saint-Herblain 44807, France

^b Bureau Veritas, Research Department, Paris 92937, France

^c Ecole Centrale Nantes, GeM Institute UMR 6183 CNRS, Nantes 44321, France

Slamming-induced whipping is traditionally computed as the response of a linear-elastic structural model. However, in order to investigate the consequence of whipping on the hull girder's collapse, the hydro-structure interaction must be performed in a fully-coupled approach where the nonlinearities of both domains are considered. Therefore, this paper presents a new approach developed for solving the fully-coupled hydroelastoplastic problem. The structural part is modeled as two non-uniform Timoshenko beams, connected with a nonlinear hinge, described by the nonlinear relation between the internal bending moment and the relative rotation angle. The hydrodynamic problem is solved using the 3D boundary element method, and the exact coupling between the structural and the 3D hydrodynamic models is achieved by constructing the hydrodynamic boundary value problem for each shape function of the finite element beam model. The hydroelastoplastic response is calculated using a hybrid nonlinear time-domain approach, allowing for very fast computation of the nonlinear whipping response. Finally, the nonlinear whipping response is calculated on a broad range of ships and it is compared to the linear whipping response in order to derive the whipping effectiveness coefficients. It is shown that the nonlinear structural behavior has a very small influence on the whipping response, and thus, the effectiveness of whipping should not be reduced.

1. Introduction

The modern world is driven by the need for safe, environmentally friendly, and economical ship designs; in consequence, the prediction of wave-induced motions and loads is of paramount importance. The classic seakeeping methods used for computing the hydrodynamic responses of a ship are based on the assumption that structural deformations are small, and consequently, the ship is considered as a rigid body. This leads to the so-called quasi-static approach for evaluating the structural response, where the effects of the structural dynamics (ship vibrations) are neglected. This approach works well as far as the response of the structural natural modes is not dynamically amplified, which is the case most often in practice, but not always. For the cases where the dynamic amplification of the structural response is important, the full coupling of the hydrodynamic loading and the structural response is required. As far as the global structural response is concerned, two main physical phenomena are of concern: springing and whipping. The springing is a resonant phenomenon and represents the entertained hull vibrations induced by the continuous action of

the wave loading, while the whipping represents the transient hull vibrations induced by the impulsive hydrodynamic loading (slamming, green water, etc.). Due to its resonant character, the springing response becomes significant only when the excitation frequencies are close to the frequencies of the structural natural modes. Contrary to springing, the whipping is mainly driven by the nature of the impulsive loading, which is usually independent of the structural natural frequencies. This means that any floating body can be potentially affected if the ratio of the impulsive loading duration and the structural natural period is critical. In the case of ultra-large container ships (ULCS), the natural frequencies are usually low (few seconds), and at the same time, the slamming loads are important (large bow flare combined with the relatively high ship speed). Hence, ULCS are prone to both springing and whipping types of hydroelastic responses. Only the whipping phenomenon is of concern in this paper.

The preliminary investigations by Bishop and Price (1979) fostered an understanding of the physical phenomena behind the hydroelasticity of ships. Since then, several more or less sophisticated models were

* Corresponding author.

E-mail address: george.jagite@bureauveritas.com (G. Jagite).

proposed, where the hydroelastic problem is solved at different levels of complexity and accuracy.

One of the well-established methods was proposed by Tuitman and Malenica (2009), and it solves the fully coupled hydroelastic problem by making use of the generalized modes approach. The natural modes can be calculated either using a one-dimensional (1D) beam model or the full three-dimensional (3D) Finite Element Method (FEM) model of the ship structure. After solving the general seakeeping problem in the frequency-domain using a 3D Boundary Element Method (BEM) based on Green's sources, the time-domain simulation is performed following the approach proposed by Cummins (1962). Aside from that, several nonlinear effects are added, such as the Froude-Krylov correction and the slamming loads, which are calculated using the Generalized Wagner Model (GWM) (Wagner, 1932; De Lauzon et al., 2015). The method allows for the computation of springing and whipping responses, and was validated with both experimental and full-scale results (Derbanne et al., 2010). More recently, Kim et al. (2013) developed a similar fully coupled hydroelastic method. In their method, the hydrodynamic problem is solved using a B-Spline 3D Rankine panel method, while the structural model can also be either a 1D or a 3D FEM model; the slamming loads are also determined using the GWM. The coupling between the structural and the hydrodynamic model is made directly, which allows direct access to the structural responses at any required position. The method showed good results when compared with the model tests (Kim et al., 2014).

Nevertheless, the Computational Fluid Dynamics (CFD) techniques have evolved significantly in the past decade. Seng (2012) developed a numerical method for computing the springing and slamming-induced whipping responses of a ship using OPENFOAM (an open-source CFD package, Weller et al. (1998)). The structural part was modeled as a classical non-uniform Timoshenko beam model, and the transfer of the displacement and fluid forces was performed using the modal spaces. The procedure developed by Seng (2012) agreed satisfactorily with model tests and showed the potential to accurately predict the global hydroelastic responses using the so-called field methods (Seng et al., 2014). The prediction of extreme loads, including wave-induced vibrations, using numerical solutions of the Reynolds-averaged Navier-Stokes equations has also been reported by Oberhagemann et al. (2015).

More recently, several researchers investigated the hydroelastic response using fully-coupled CFD-FEA (Finite Element Analysis), for example, Lakshminarayanan and Temarel (2018) and Seng et al. (2018). Takami and Iijima (2019) investigated the combined global and local hydroelastic response in a large container ship based on two-way coupled CFD and FEA. For the hydrodynamic part, they adopted a commercial solver, named STAR-CCM+; while the structural part is modeled as a 3D Finite Element (FE) model, and the FEA solver of choice was the dynamic explicit solver implemented in LS-DYNA. The two-way coupling is performed in a staggered manner and shows a reasonable agreement with the experimental data. However, the cost of running a two-way strongly coupled simulation is very high: 30 h per physical 10 s in full scale on a modern workstation.

In the aforementioned methods and investigations, as well as in the works reported in the extensive literature reviews by Chen et al. (2006), Hirdaris and Temarel (2009) and Temarel et al. (2016), Ergin et al. (2018), the structural behavior is always treated as linear and elastic. However, the real structural behavior is nonlinear elastic-plastic. This means that when a ship is subjected to an extreme loading scenario, the hull girder might suffer from local buckling or plastic deformations, comporting different than the linear elastic assumption.

Moreover, it should be mentioned that after the two accidents: MSC Napoli and MOL Comfort (Branch, 2008; ClassNK, 2014), the importance of whipping on the extreme hull girder loads has received much attention, but its consequences on the hull girder's collapse are still unclear. The most common practice to evaluate the ultimate strength of a relatively flexible floating structure is to compare the maximum

dynamic vertical bending moment (VBM) after a slamming event, which is derived from hydroelastic calculations, with the quasi-static hull girder capacity; where the quasi-static hull girder ultimate strength is determined either by simplified methods such as the "Smith" method, or by some more advanced methods such as idealized structural unit method, or nonlinear finite element method (Smith, 1977; Ueda and Rashed, 1984; Paik et al., 2008).

Some aspects regarding the current procedure remain unclear, for example the influence of the dynamic effects associated with the whipping-induced stresses, or the capability of the current hydroelastic methods to accurately predict the extreme dynamic response on the basis of a linear elastic structural model.

The first aspect was previously investigated by the authors, and it was found that the dynamic factors are having a minimal effect over the structural capacity. The comprehensive analyses of the dynamic ultimate strength for stiffened panels can be found in Jagite et al. (2019a) and Jagite et al. (2020b); while the analyses of the dynamic hull girder ultimate strength are presented in Jagite et al. (2019b) and Jagite et al. (2020a).

The second aspect represents the starting point of the research work presented in this paper, aiming at analyzing the influence of the nonlinearities existing in the structural model over the slamming-induced whipping response. Thus, the hydroelastic problem transforms into a hydroelastoplastic problem. In the hydroelastoplasticity of ships, the structural behavior is nonlinear, including material and geometric nonlinearities.

A preliminary investigation on the hydroelastoplastic response of a ship subjected to slamming induced whipping was reported by Dow (1981). They developed a numerical model that considers the ship as 21 lumped masses connected by beam elements. The lumped masses included the hydrodynamic added mass of the first elastic mode. For the structural part, only four of the total beam elements were enforced with a precomputed moment-curvature behavior; others kept a purely elastic behavior. Dow (1981) applied a short impulse load (0.05 s), near the fore-end of the ship, which was supposed to represent the bottom impact slamming. Their preliminary results showed that the hull girder capacity was increased by about 70%–95% when short impulsive loads were applied. However, Dow (1981) acknowledged that the loading scenarios considered were not representing the reality, and more realistic scenarios should be considered, where the high-frequency loads (whipping) are combined with the low-frequency loads (wave loads), and with the still water component.

About 30 years later, Iijima et al. (2011) investigated the dynamic collapse of a ship's hull girder in waves, having a focus on the post-ultimate strength behavior. In their model, the hydrodynamic problem was solved by making use of the nonlinear strip theory, while the structural part was considered as two rigid bodies connected to each other by a nonlinear rotational spring. The numerical model was validated against several experimental investigations that considered both structural and hydrodynamic similarities. The model developed by Iijima et al. (2011) shows the capability of following a precomputed moment-curvature behavior and computes the severity of the collapse under large single wave loads. Several similar investigations on the post-collapse behavior of the ship's hull girder have been reported by Xu et al. (2011), Iijima and Fujikubo (2012, 2015) and Iijima and Fujikubo (2018). It is worth mentioning that the recent studies considered the hull girder as two elastic beams connected by a nonlinear rotational spring, and the hydrodynamic problem being solved by making use of the boundary element method. However, the structure is subjected only to low-frequency loads, and none of these investigations are taking into account the slamming-induced whipping response. Other researchers investigated the behavior of very-large floating structures (VLFS) in waves, for example: Yoon and Lee (2017) and Iida and Umazume (2020).

As previously mentioned, this research work aims to analyze the influence of the nonlinear structural behavior over the slamming-induced

whipping response. Hitherto, to the authors' knowledge, there is no software capable of computing the nonlinear whipping response of ships. Moreover, only a minimal number of publications are focused on this aspect. Derbanne et al. (2016) presented a simplified method to investigate the dynamic hull girder response by considering the nonlinear effect of hull girder ultimate strength. The numerical model is the well-known single degree of freedom vibration model, which can take different moment–curvature relation curves and different hydrodynamic loading sequences. From the hydrodynamic point of view, the model deals with realistic loading scenarios, including the still water bending moment, the wave bending moment, and a slamming load. Derbanne et al. (2016) introduced the dynamic ultimate capacity factor as the maximum allowable linear whipping response on a scenario where the nonlinear whipping response reaches the failure point, divided by the quasi-static ultimate capacity. It was shown that the dynamic ultimate capacity factor is highly dependent on the nonlinear model of the hull girder behavior. However, it is always greater than unity, meaning that the linear dynamic response of the hull girder can exceed the quasi-static ultimate capacity without reaching the failure point. In conclusion, Derbanne et al. (2016) pointed out the necessity of using real loading sequences and showed that simple loading scenarios, as pure slamming impacts on still water, will overestimate the dynamic ultimate capacity factor.

Yamada (2019) investigated the possibility of using a commercial 3D FEM solver to simulate the dynamic elastic–plastic whipping response of the hull girder of a large container ship due to slamming load. The full FE model of a container ship has been subjected to a series of time-domain simulations where the slamming load is applied to the fore-end. In addition to the slamming load, the still water pressure has been considered, but the wave loads are missing. Besides, the model is not considered as a free-floating body, as in a realistic scenario, but it is simply supported on the aft end. Also, the slamming load is balanced either by using the inertia relief method or using an initial rotational velocity. These aspects are making the method developed by Yamada (2019) as being far from the real physical mechanism of the slamming induced whipping response. Therefore, the proposed methodology will not yield correct information on the dynamic elastic–plastic response of ships.

In light of the above, we delve into the nonlinear whipping response using a broad range of ships. Numerical investigations are carried out using the methodology presented by the authors in the previous paper (Jagite et al., 2020c). Within this method, the nonlinear whipping response is computed by solving the fully-coupled hydroelastoplastic problem. A brief description of the method is presented in Section 2. The main particulars of the considered ships are depicted in Section 3. In Section 4, the nonlinear whipping response (i.e., using a nonlinear structural behavior) is compared with the linear whipping response (i.e., using a linear elastic structural model) in order to derive the dynamic ultimate capacity factor, as the maximum allowable linear whipping response on a scenario where the nonlinear whipping response reaches the failure point, divided by the quasi-static ultimate capacity. At last, concluding remarks are discussed in Section 5.

2. Fully-coupled hydroelastoplastic model

The overall procedure for the hydroelastoplastic calculations was presented in Jagite et al. (2020c), and here below, we just briefly recall the basic principles. It is important to mention that whipping is by nature always “nonlinear” from the hydrodynamic point of view, the distinction between “linear” and “nonlinear” in this paper pertains to the structural model.

2.1. Structural model

At first, it is essential to mention that in real cases, only a very limited extent of the structure collapses, as previously shown in (Matsumoto et al., 2016; Jagite et al., 2019b). The collapse area associated with a “weak frame” in the hull girder can be concentrated at a node of the finite element beam model. Therefore, the ship is modeled as two non-uniform Timoshenko beams connected via a nonlinear hinge, as exhibited in Fig. 1.

The total number of elements is $n_{elem} = n_1 + n_2$, where n_1 and n_2 are the number of elements for the first and second beam, respectively. Each node has two degrees of freedom (DOF-s) for the vertical displacement w_i and rotation θ_i . The nodes are defined at the neutral axis of the ship. Since the hull girder stiffness in axial direction is significantly bigger than the bending stiffness, the nodal axial displacements are included in the FE model. Instead, a global rigid-body DOF for the ship's surge motion is defined at the center of gravity of the ship.

The equation of motion for the structural problem can be written in the compact form as follows:

$$\mathbf{m}\ddot{\mathbf{x}}(t_{n+1}) + \mathbf{b}\dot{\mathbf{x}}(t_{n+1}) + \mathbf{c}\mathbf{x}(t_{n+1}) = \mathbf{F}(t_{n+1}) \quad (1)$$

where the global matrices for mass \mathbf{m} , damping \mathbf{b} and stiffness \mathbf{c} contain the assembled mass, damping and stiffness matrices, for the first and the second beam, respectively. Besides, the coupling terms for the surge-pitch motions are included in the global mass matrix \mathbf{m} , as described in Jagite et al. (2020c). \mathbf{x} is the vector of displacements and $\dot{\mathbf{x}}$, $\ddot{\mathbf{x}}$ are the velocity and acceleration vectors; \mathbf{F} is the vector of external nodal forces.

The nonlinear hinge is modeled as two coincident nodes, where the additional rotation due to the collapse is represented as the relative rotation between the two rotational DOF-s: θ_L associated to the aft part of the model, and θ_R associated to the fore part of the model. In the numerical model the hinge's behavior is defined using a set of Lagrange multipliers. This aspect will be discussed later in this paper.

The nonlinear behavior of this hinge is described by the nonlinear relation between the internal bending moment and the relative rotation angle, i.e., the well-known moment–curvature curve used to describe the ultimate strength of a ship section. The hinge's behavior can be precalculated since the dynamic effects have a minimal influence on the ultimate strength of a ship section (as shown in Jagite et al. (2019b)), and can be obtained either from:

- (i) the analytical method known as “Smith method”;
- (ii) a nonlinear FE analysis (NL-FEA) using the 3D FEM model of a “slice” of the hull girder; a static arc-length analysis procedure is preferred in order to capture the “post-collapse” part of the characteristic.

When the nonlinear behavior is calculated with one of the above-mentioned methods, the raw output is always the relationship between the internal bending moment M_{int} and the total rotation over a model's length L . A typical moment versus total rotation angle is depicted in Fig. 2(a). The total rotation angle θ includes a linear part associated to the extend L of the model and a nonlinear associated with the collapse area, which can be considered as independent of L , as previously described in Jagite et al. (2020c). Therefore, in order to avoid the situation where the hull girder's linear elastic behavior is taken twice into account (i.e., once in the adjacent beam elements and once in the hinge itself) the linear part must be removed from the precomputed nonlinear behavior, as Fig. 2(b) bears out. Hence, the modified nonlinear hinge behavior is represented by the relationship between the internal bending moment M_{int} , and the plastic rotation relative plastic rotation angle θ_p . The plastic rotation angle is computed as the difference between the total rotation angle, and the linear rotation angle (for more details see Jagite et al. (2020c)).

In Fig. 2 the ultimate strength is noted as M_U and represents the maximum point on the curve. Aside from that, the failure point is noted as θ_f . The failure point can be defined as the relative plastic rotation angle obtained at the moment when the ultimate strength is reached.

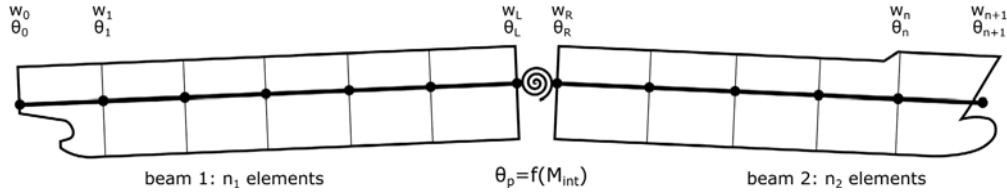


Fig. 1. Hull girder model including a nonlinear hinge.

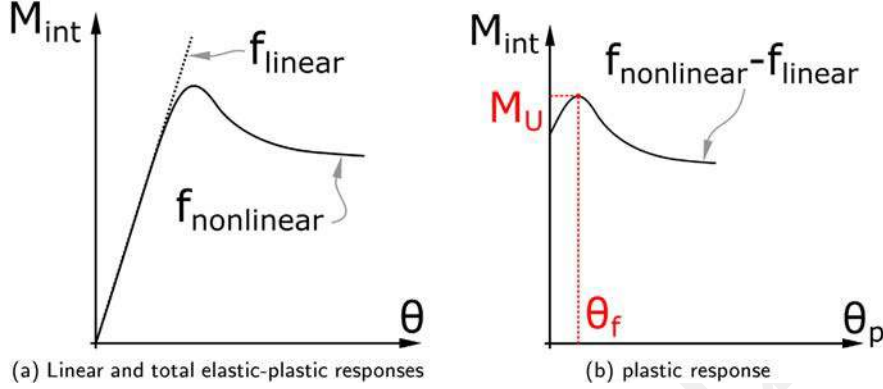


Fig. 2. Characteristic modification for the nonlinear hinge.

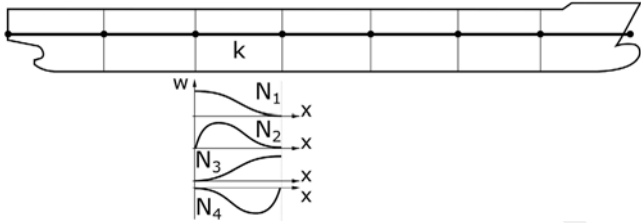


Fig. 3. Illustration of the ship's beam finite element model and the shape functions.

2.2. Hydrodynamic model

The exact coupling between the finite beam element of the structure and the 3D hydrodynamic model is achieved by constructing the hydrodynamic boundary value problems (BVP-s) for each shape function of the finite elements, hence, for each degree of freedom, as proposed by Malenica (1998). Aside from that, a supplementary BVP is defined for the global rigid-body mode defined for the surge motion.

For an isolated finite element k the shape functions are illustrated in Fig. 3. The methodology for projecting the shape functions on the hydrodynamic mesh is presented in detail in Jagite et al. (2020c). It is important to mention that the total number of BVP-s defined is $n_{mod} = 4 \cdot n_{elem} + 1$. This means that in addition to the modes represented by each element's shape functions, a global rigid-body mode for surge motion is defined.

The hydrodynamic problem is considered within the usual assumptions of the potential flow, and the complex BVP-s are solved for a range of frequencies yielding the hydrodynamic coefficients in terms of added mass, wave damping, and wave excitation. Within the present research work the frequency-domain seakeeping problem is solved by using a 3D BEM based on the pulsating Green's sources available in the commercial software HYDROSTAR, which is developed and maintained by Bureau Veritas.

Keeping in with the desire of predicting the nonlinear structural response of a ship subjected to slamming loads, it is necessary to perform the calculations in the time-domain. Instead of solving directly

the time-domain hydrodynamic problem, which can be extremely expensive, one well-known solution is the hybrid nonlinear time-domain method. This basically means that the time-dependent diffraction force is calculated using the complex response amplitude operators (RAO-s) for the diffraction force calculated in the frequency-domain. The radiation force is calculated from the memory-response functions and the history of velocities. In addition, the nonlinear loads due to slamming are computed using the Modified Logvinovich Model (MLM) (Korobkin, 2004; Korobkin and Malenica, 2005). The slamming pressures are determined analytically over several two-dimensional (2D) sections defined on the fore extremity of the ship. These 2D sections are created by cutting the 3D hydrodynamic mesh with several oblique planes. The resulting 2D slamming pressures are firstly integrated over the 3D hydrodynamic mesh and later transferred to the nodes of the FE model (for more details, please refer to Jagite (2020)).

Thus, the equation of motion in time-domain resembles the usual equation, with the addition of the convolution integral over the past history for the velocity, as presented by Cummins (1962):

$$(\mathbf{A}(\infty) + \mathbf{m})\ddot{\mathbf{x}}(t_{n+1}) + \mathbf{b}\dot{\mathbf{x}}(t_{n+1}) + \int_0^{t_{n+1}} \mathbf{K}(t_{n+1} - \tau)\dot{\mathbf{x}}(\tau)d\tau + (\mathbf{C} + \mathbf{c})\mathbf{x}(t_{n+1}) = \mathbf{F}(t_{n+1}) + \mathbf{Q}(\mathbf{x}, \dot{\mathbf{x}}, t_{n+1}) \quad (2)$$

where $\mathbf{A}(\infty)$ represents the infinite frequency added mass matrix, and $\mathbf{K}(t)$ represents the matrix of impulse response functions. On the right-hand side, the force vector \mathbf{F} is composed of the diffraction force \mathbf{F}_{DI} , the force due to gravity acceleration \mathbf{F}_G , and the force due to still water pressure \mathbf{F}_{SW} . The vector $\mathbf{Q}(\mathbf{x}, \dot{\mathbf{x}}, t_{n+1})$ represents the nonlinear slamming force, which depends on the relative motion and the velocities of the fore extremity. This simply means that the slamming force at instant t_{n+1} depends on the response at instant t_{n+1} , and vice-versa. As a consequence, the equation of motion presented in Eq. (2) describes a coupled nonlinear problem.

As previously mentioned in Section 2.1, the nonlinear hinge is modeled as two coincident nodes, and its behavior is defined using a set of Lagrange multipliers. The conditions that are to be imposed using a set of Lagrange multipliers are:

- (i) the linear surge motion in order to handle the horizontal motions of the ship;

- (ii) the continuity of the vertical displacement field at the nonlinear hinge, which can be seen as: $w_L - w_R = 0$;
- (iii) the nonlinear behavior of the hinge, which can be seen as: $\theta_L - \theta_R = \theta_d = f(M_{int})$, and must follow the precomputed behavior.

The first condition enforces the linear surge motion obtained by performing inverse Fourier transform on the linear frequency-domain results. The second condition specifies that the vertical displacement field along the ship is continuous. Hence, the vertical displacement at the last node of the aft beam and the vertical displacement at the first node of the fore beam must coincide. The third condition defines the discontinuity in the rotation field at the nonlinear hinge position to model the “collapsing” frame in the hull girder under extreme scenarios. The discontinuity in the rotation field at time instant t_{n+1} depends on the internal bending moment at the nonlinear hinge position at the same instant t_{n+1} , and vice-versa. This nonlinear relationship must follow the precomputed nonlinear hinge behavior, defined in Fig. 2.

As a consequence, the total number of DOF-s increases with the number of Lagrange multipliers defined. The notation *tilde* ($\tilde{\cdot}$) has been adopted to differentiate the components whose size was increased. Furthermore, the constraints to be imposed can be written in a matrix form as: $\mathbf{B}_{\tilde{\mathcal{C}}} \cdot \mathbf{x} = \mathbf{h}$. Thus, one could include the boundary condition matrix $\mathbf{B}_{\tilde{\mathcal{C}}}$, and its transpose in the enhanced stiffness matrix, $\tilde{\mathbf{c}}$, as follows:

$$\tilde{\mathbf{c}} = \begin{bmatrix} \mathbf{c} & \mathbf{B}_{\tilde{\mathcal{C}}}^T \\ \mathbf{B}_{\tilde{\mathcal{C}}} & \mathbf{0} \end{bmatrix}, \quad \tilde{\mathbf{x}}(t_{n+1}) = \begin{bmatrix} \mathbf{x}(t_{n+1}) \\ \lambda(t_{n+1}) \end{bmatrix}, \quad \tilde{\mathbf{F}}(t_{n+1}) = \begin{bmatrix} \mathbf{F}(t_{n+1}) \\ \mathbf{h}(t_{n+1}) \end{bmatrix} \quad (3)$$

The vectors \mathbf{h} and λ can be seen as:

$$\mathbf{h}(t_{n+1}) = [u_{x_{lin}}(t_{n+1}) \quad 0 \quad \theta_d(BM_d(t_{n+1}))]^T, \quad (4)$$

$$\lambda = [F_x(t_{n+1}) \quad SF_d(t_{n+1}) \quad BM_d(\theta_d(t_{n+1}))]^T$$

where $u_{x_{lin}}$ is the linear surge motion obtained by performing inverse Fourier transform on the linear frequency-domain results, F_x represents the force necessary to handle the horizontal motions of the ship. SF_d represents the internal vertical shear force applied from the right node to the left node in order to enforce the continuity of the vertical displacement at the location of the nonlinear hinge. $BM_d(\theta_d(t_{n+1}))$ represents the internal vertical bending moment between the degrees of freedom denoted θ_L and θ_R , and depends on the relative plastic rotation angle $\theta_d(BM_d(t_{n+1}))$

For all other components where the notation *tilde* appears, the size of those vectors or matrices was increased by adding zeros on the additional lines and/or columns. Finally, the nonlinear equation of motion for solving the fully-coupled hydroelastoplastic problem becomes:

$$(\tilde{\mathbf{A}}(\infty) + \tilde{\mathbf{m}})\ddot{\tilde{\mathbf{x}}}(t_{n+1}) + \tilde{\mathbf{b}}\dot{\tilde{\mathbf{x}}}(t_{n+1}) + \int_0^{t_{n+1}} \tilde{\mathbf{K}}(t_{n+1} - \tau)\dot{\tilde{\mathbf{x}}}(\tau)d\tau + (\tilde{\mathbf{C}} + \tilde{\mathbf{c}})\tilde{\mathbf{x}}(t_{n+1}) = \tilde{\mathbf{F}}(t_{n+1}) + \tilde{\mathbf{Q}}(\mathbf{x}, \dot{\mathbf{x}}, t_{n+1}) \quad (5)$$

2.3. Numerical time-integration

Within the present research work, it was decided to employ the Hilber-Hughes-Taylor (HHT) scheme (Hilber et al., 1977) for solving the 2nd order ordinary differential equation which describes the equation of motion. According to HHT scheme, the discretized equation of motion, presented in Eq. (5), can be written as:

$$\begin{aligned} & (\tilde{\mathbf{A}}(\infty) + \tilde{\mathbf{m}})\ddot{\tilde{\mathbf{x}}}(t_{n+1}) + (1 + \alpha) \left(\tilde{\mathbf{b}}\dot{\tilde{\mathbf{x}}}(t_{n+1}) + \int_0^{t_{n+1}} \tilde{\mathbf{K}}(t_{n+1} - \tau)\dot{\tilde{\mathbf{x}}}(\tau)d\tau + (\tilde{\mathbf{C}} + \tilde{\mathbf{c}})\tilde{\mathbf{x}}(t_{n+1}) \right) - \\ & \alpha \left(\tilde{\mathbf{b}}\dot{\tilde{\mathbf{x}}}(t_n) + \int_0^{t_n} \tilde{\mathbf{K}}(t_n - \tau)\dot{\tilde{\mathbf{x}}}(\tau)d\tau + (\tilde{\mathbf{C}} + \tilde{\mathbf{c}})\tilde{\mathbf{x}}(t_n) \right) \\ & = (1 + \alpha) (\tilde{\mathbf{F}}(t_{n+1}) + \tilde{\mathbf{Q}}(t_{n+1})) - \alpha (\tilde{\mathbf{F}}(t_n) + \tilde{\mathbf{Q}}(t_n)) \end{aligned} \quad (6)$$

where α can vary between $[-1/2, 0]$. The smaller the value of α , the more damping is induced in the numerical solution. Hence, a value of $\alpha =$

-0.05 is used in order to include a slight amount of numerical damping, as recommended for a transient-fidelity structural response (ABAQUS, 2017).

Furthermore, Eq. (6) is solved numerically by making use of Newmark's equations (Newmark et al., 1959) in order to write the vectors of accelerations and velocities as function of displacements. Then, the displacement at time t_{n+1} , at iteration i can be approximated by a linearized expression of the form $\tilde{\mathbf{x}}^{(i)}(t_{n+1}) = \tilde{\mathbf{x}}^{(i-1)}(t_{n+1}) + \Delta\tilde{\mathbf{x}}$.

The nonlinear problem is solved using Newton-Raphson scheme to minimize the vector of residuals. Thus, the equation of motion at iteration i at time t_{n+1} can be expressed in the following effective form:

$$\mathbf{K}_E^{(i)} \cdot \Delta\tilde{\mathbf{x}} = \mathbf{F}_E^{(i)} \quad (7)$$

where $\mathbf{K}_E^{(i)}$ is the effective stiffness matrix:

$$\mathbf{K}_E^{(i)} = (\tilde{\mathbf{A}}(\infty) + \tilde{\mathbf{m}}) \frac{1}{\beta \Delta t^2} + (1 + \alpha) \left(\frac{\gamma}{\beta \Delta t} \left(\tilde{\mathbf{b}} + \frac{1}{2} \tilde{\mathbf{K}}[0] \right) + \tilde{\mathbf{C}} + \tilde{\mathbf{c}} \right) \quad (8)$$

and $\mathbf{F}_E^{(i)}$ is the effective force vector:

$$\begin{aligned} \mathbf{F}_E^{(i)} = & (1 + \alpha) \left(\tilde{\mathbf{F}}^{(i)}(t_{n+1}) + \tilde{\mathbf{Q}}^{(i)}(t_{n+1}) \right) - \alpha \left(\tilde{\mathbf{F}}(t_n) + \tilde{\mathbf{Q}}(t_n) \right) \\ & - (\tilde{\mathbf{A}}(\infty) + \tilde{\mathbf{m}})\ddot{\tilde{\mathbf{x}}}^{(i-1)}(t_{n+1}) \\ & - (1 + \alpha) \left(\tilde{\mathbf{b}}\dot{\tilde{\mathbf{x}}}^{(i-1)}(t_{n+1}) + \int_0^{t_{n+1}} \tilde{\mathbf{K}}(t_{n+1} - \tau)\dot{\tilde{\mathbf{x}}}(\tau)d\tau \right) \\ & + \alpha \left(\tilde{\mathbf{b}}\dot{\tilde{\mathbf{x}}}(t_n) + \int_0^{t_n} \tilde{\mathbf{K}}(t_n - \tau)\dot{\tilde{\mathbf{x}}}(\tau)d\tau \right) \\ & - (1 + \alpha)(\tilde{\mathbf{C}} + \tilde{\mathbf{c}})\tilde{\mathbf{x}}^{(i-1)}(t_{n+1}) + \alpha(\tilde{\mathbf{C}} + \tilde{\mathbf{c}})\tilde{\mathbf{x}}(t_n) \\ & - \left((\tilde{\mathbf{A}}(\infty) + \tilde{\mathbf{m}})\Delta\ddot{\tilde{\mathbf{x}}} + (1 + \alpha) \left(\left(\tilde{\mathbf{b}} + \frac{1}{2} \tilde{\mathbf{K}}[0] \right) \dot{\tilde{\mathbf{x}}} + \tilde{\mathbf{C}} + \tilde{\mathbf{c}}\Delta\tilde{\mathbf{x}} \right) \right) \end{aligned} \quad (9)$$

Nonetheless, the predictions made at iteration $i = 0$ can be seen as:

$$\begin{aligned} \tilde{\mathbf{x}}^{(0)}(t_{n+1}) &= \tilde{\mathbf{x}}(t_n) + \Delta t \dot{\tilde{\mathbf{x}}}(t_n) + (0.5 - \beta) \Delta t^2 \ddot{\tilde{\mathbf{x}}}(t_n), \\ \dot{\tilde{\mathbf{x}}}^{(0)}(t_{n+1}) &= \dot{\tilde{\mathbf{x}}}(t_n) + (1 - \gamma) \Delta t \ddot{\tilde{\mathbf{x}}}(t_n), \quad \ddot{\tilde{\mathbf{x}}}^{(0)}(t_{n+1}) = 0 \end{aligned} \quad (10)$$

and the corrections for iteration i can be seen as:

$$\begin{aligned} \tilde{\mathbf{x}}^{(i)}(t_{n+1}) &= \tilde{\mathbf{x}}^{(i-1)}(t_{n+1}) + \Delta\tilde{\mathbf{x}}, \quad \dot{\tilde{\mathbf{x}}}^{(i)}(t_{n+1}) = \dot{\tilde{\mathbf{x}}}^{(i-1)}(t_{n+1}) + \gamma \Delta\dot{\tilde{\mathbf{x}}}/\beta \Delta t, \\ \ddot{\tilde{\mathbf{x}}}^{(i)}(t_{n+1}) &= \ddot{\tilde{\mathbf{x}}}^{(i-1)}(t_{n+1}) + \Delta\ddot{\tilde{\mathbf{x}}}/\beta \Delta t^2 \end{aligned} \quad (11)$$

The logical scheme for solving the coupled hydroelastoplastic problem is depicted in Fig. 4. At each time step, two iterative loops are necessary to handle the nonlinearities. On the one hand, the inner-iterations, indicated with blue lines, are for computation of the nonlinear loads (i.e., slamming). On the other hand, the outer-iterations, indicated with red lines, are for the nonlinear structural behavior. The nonlinear structural problem is solved in such way that at each event when the internal bending moment exceeds the yield limit, the discontinuity angle is gradually increased until the new solution $(\theta_d^{(j)}, BM_{disc}^{(j)})$ follows the precomputed behavior. For more details on the nonlinear algorithm please refer to Jagite et al. (2020c).

The computation stops when the end time is reached, or when the structural failure is reached. The failure is reached when the relative plastic rotation angle becomes higher or equal to the failure point: $\theta_d \geq \theta_f$.

3. Ship database

The newly developed hydroelastoplastic model is employed in the analysis of the nonlinear whipping response in head waves. In the current research work, it was decided to use fourteen container ships ranging from 160 m to 350 m. The principal characteristics are presented in Table 1, where L_{BP} represents the length between perpendiculars, B represents the molded breadth of the ship, D and T are the construction depth and the draft, respectively. The cargo-carrying capacity, expressed in terms of TEU (twenty-foot equivalent unit), is denoted as CC . The block coefficient of the ship is indicated as c_B . The

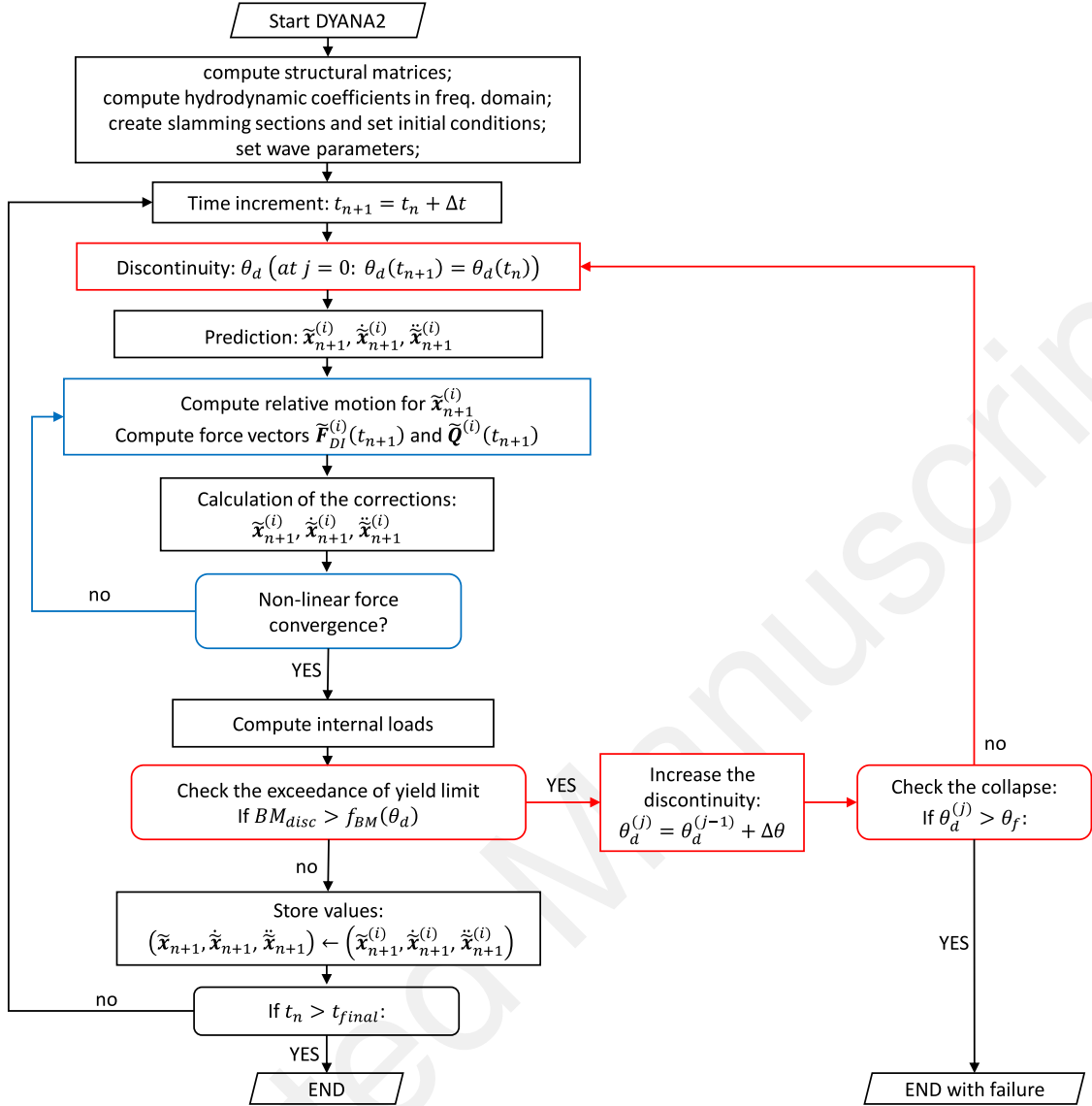


Fig. 4. Computation scheme for solving the nonlinear hydroelastoplastic problem.

wet natural frequencies for the first two vertical vibrational modes are shown on the 1st ν_b and 2nd ν_b columns. Moreover, the last two columns are showing the allowable still-water bending moment in hogging at midship (M_{SW}), and the ultimate hogging bending moment (M_U), respectively.

From the data exhibited in Table 1 it can be seen that with the increase in length, as well as with the increase in cargo-carrying capacity, the frequencies of the eigenmodes decreases, indicating that bigger ships are more flexible. Besides, we can observe that an important loading component for container ships is represented by the still-water bending moment. For the hogging condition, the still-water bending moment is about 30% of the ultimate strength. Hence, it is extremely important to consider realistic loading scenarios when analyzing the nonlinear whipping response.

3.1. Nonlinear hinge behavior

This section presents the calculation of the nonlinear hinge behavior for all fourteen container ships. As previously mentioned in Section 2.1, two different methods can be used to determine the hinge's behavior:

Table 1
Principal characteristics of ships.

Ship	L_{BP} [m]	B [m]	D [m]	T [m]	c_B	CC [TEU]	1 st ν_b [Hz]	2 nd ν_b [Hz]	M_{SW} [GNm]	M_U [GNm]
S01	160.0	27.0	14.0	8.8	0.700	1600	0.917	1.951	0.72	2.75
S02	160.0	27.0	14.0	9.2	0.700	1600	1.190	2.566	0.72	2.75
S03	170.0	24.0	12.0	5.5	0.730	1700	0.886	1.939	0.89	2.61
S04	170.0	30.0	16.0	11.0	0.610	2000	1.050	2.240	0.77	3.49
S05	185.0	30.0	16.0	11.0	0.673	2100	0.838	1.803	1.04	4.55
S06	205.0	31.0	19.0	11.0	0.639	2500	0.923	1.953	1.42	6.30
S07	260.0	32.0	21.0	12.0	0.678	4500	0.540	1.157	2.94	9.95
S08	270.0	40.0	24.0	12.5	0.626	5900	0.591	1.218	3.87	12.50
S09	285.0	32.0	22.0	13.5	0.684	5000	0.606	1.306	3.04	10.56
S10	290.0	40.0	24.0	12.0	0.630	6500	0.628	1.312	4.41	13.92
S11	320.0	43.0	25.0	13.0	0.675	8600	0.491	1.035	6.20	19.01
S12	330.0	43.0	27.0	13.0	0.688	9300	0.485	1.027	6.86	20.72
S13	345.0	45.0	30.0	15.5	0.689	12000	0.529	1.094	7.06	23.52
S14	350.0	51.0	30.0	15.5	0.720	14000	0.437	0.903	8.73	27.72

3.1.1. Using “Smith” method

The ultimate capacity curves in hogging have been firstly computed using the simplified method based on the “Smith” approach, available

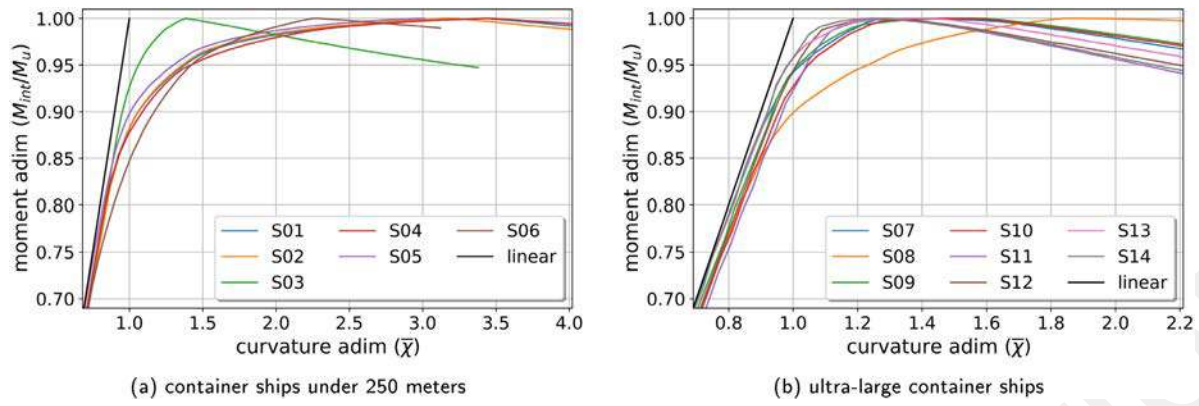


Fig. 5. Bending moment vs. curvature curve for fourteen container ships.

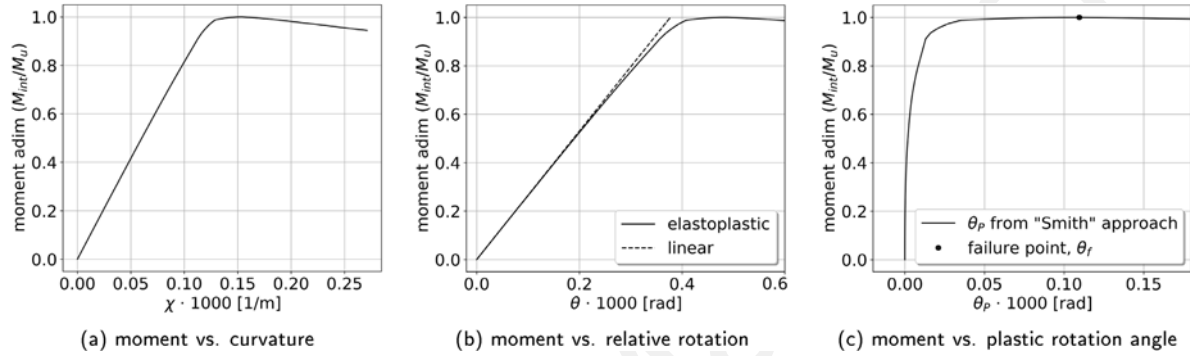


Fig. 6. Transformation of typical moment vs. curvature behavior, from Smith approach, to moment vs. plastic rotation angle (results obtained for S12).

in MARS2000 software (Veritas, 2019c). The moment versus curvature curves are non-dimensionalized in such a way that for each ship the non-dimensional curvature $\bar{\chi}$ is equal to one when the linear bending moment versus ultimate strength ratio is equal to unity, as Fig. 5(b) bears out. On the one hand, it is observed that smaller ships, under 200 m, have a higher failure point $\bar{\chi}$, varying between 2.3 and 3.2, as shown in Fig. 5(a). On the other hand, the failure point for typical ULCS ranges between 1.2 and 1.4, with an exception for S08, where the failure point is equal to two, as depicted in Fig. 5(b).

As previously discussed, the behavior of the nonlinear hinge should include only the plastic part since the linear-elastic part of the stiffness is already included in the adjacent Timoshenko beam elements (Jagite et al., 2020c). Thus, it is necessary to transform the moment versus curvature curves to moment versus plastic rotation angle. At first, the total elastic-plastic rotation angle is obtained by multiplying the curvature (shown in Fig. 6(a)) with the model length $\theta = \chi L$, where L is assumed to be equal to the distance between two reinforced frames. The linear elastic rotation due to internal moment M_{int} on extent L is given by: $\theta_{linear} = M_{int}L/EI$, where EI is the bending stiffness. Therefore, the plastic rotation angle can be calculated as the difference between the elastic-plastic rotation angle and the linear-elastic one, shown in Fig. 6(b). Therefore, the moment versus plastic rotation curves based on the ‘‘Smith’’ approach are obtained, as exhibited in Fig. 6(c).

3.1.2. Using NL-FEM method

Furthermore, the nonlinear hinge behavior can be calculated using more advanced tools, based on the NL-FEM. In the current context, it was decided to create eleven NL-FEM models, each of them being extended over the one-frame bay, i.e., the distance between two reinforced frames. Ten of the models are for ships S01, S02, S05, S06, S07, S09, S10, S12, S13 and S14, having a cargo carrying capacity of 1600, 1600, 2100, 2500, 4500, 5000, 6500, 9300, 12000 and 14000 TEU, respectively. During the analysis, it was observed that bigger ships

have a smaller failure point. Thus, it was decided to create an additional model of a ULCS with the length between perpendiculars of around 380 m, and with a cargo carrying capacity of 20000 TEU. This additional ship indicated as $S_{new\ 1}$, is used to verify if the relationship between the failure point and the ship’s length is the same even for modern ULCS.

For every ship, a relatively fine mesh size is chosen; the collapse area is modeled with an average mesh size of 100 mm, while for the rest of the ship a mesh size of around 300 mm is adopted. The material behavior is defined as bi-linear elastic-plastic, including a strain hardening with a slope of 1/1000. Moreover, the initial geometric imperfections are generated as per best practice (Paik, 2018). The hull girder ultimate strength analyses are performed under enforced loads (bending moments), using the arc-length procedure. This method allows the load to be automatically increased until the ultimate capacity is reached and automatically decreased during the collapse process (ABAQUS, 2017).

The raw results obtained from the NL-FEM analyses are in terms of end-rotation angles, and internal bending moment. At first, the moment versus relative rotation curves are non-dimensionalized and presented in Fig. 7. The non-dimensionalization is done similarly as for the results obtained using the ‘‘Smith’’ approach; the non-dimensional relative rotation angle $\bar{\theta}$ equals one when the linear bending moment versus ultimate strength ratio is equal to unity. It is important to mention that the failure point calculated by NL-FEM analysis for typical ULCS ranges between 1.1 and 1.25, while the values obtained for the ships under 250 meters varies between 1.5 and 1.8. Furthermore, the nonlinear behavior can be easily transformed by removing the linear relative rotation angle from the nonlinear one, as presented in Fig. 8.

In addition, the moment versus plastic rotation angle curve for S12 obtained from NL-FEM analysis is compared in Fig. 9 with the one obtained using the simplified ‘‘Smith’’ approach. From this figure it can be observed that the failure point obtained using the simplified ‘‘Smith’’

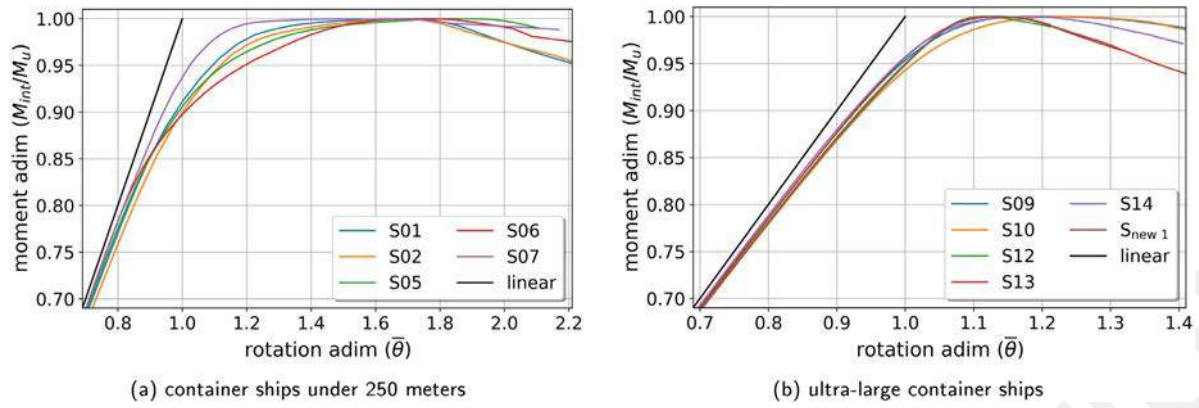


Fig. 7. Bending moment vs. relative rotation angle curves for eleven container ships.

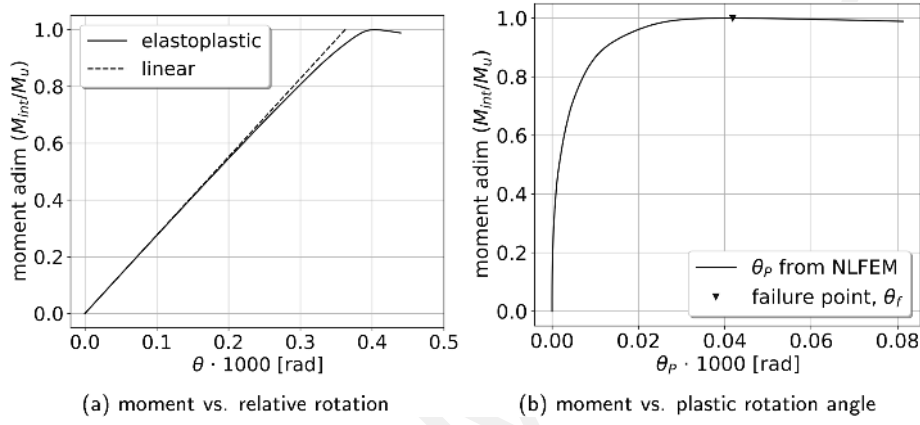


Fig. 8. Transformation of typical moment vs. relative rotation angle behavior, from NL-FEM analysis, to moment vs. plastic rotation angle (results obtained for ship S12).

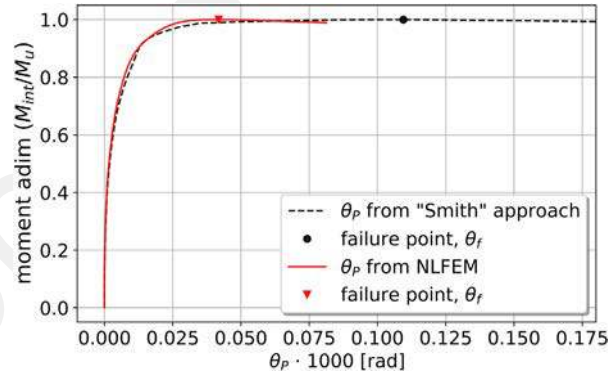


Fig. 9. Comparison of plastic rotation angle between the NL-FEM analysis and the one obtained using the "Smith" approach (results obtained for ship S12).

approach is significantly higher than the one obtained using the NL-FEM analysis. To the authors' opinion, this difference in the failure point is related to the assumption that in the "Smith" approach, the nonlinear curvature is associated with the entire length between two reinforced frames, while in the NL-FEM method the plastic strains are even more localized between two web frames (as shown in Matsumoto et al. (2016) and Jagite et al. (2019b)).

Furthermore, from Figs. 7 and 5(b) it can be seen that there is a correlation between the failure point and the ship's length. This aspect was also pointed out by Derbanne et al. (2016), showing that the location of the failure point decreases with the increase in the ships' length. Therefore, the relationship between the plastic rotation angle at the ultimate strength, denoted as θ_f , and the ships' length is presented

in Fig. 10. Thus, it is fair to say that the plastic rotation angle at the ultimate strength decreases when the length of the ship increases. Besides, it is important to point out that for ultra-large container ships over 250 meters the plastic rotation angle is relatively small.

4. Nonlinear whipping calculations

The main objective of the present research work is to determine the influence of the nonlinear structural behavior over the maximum slamming-induced whipping response on a broad range of ships, subjected to either an equivalent design wave or a design sea state. In the current investigation, the irregular wave train height is gradually scaled until the nonlinear whipping response becomes equal to the ultimate capacity, noted as M_U . If the wave signal is scaled a little bit

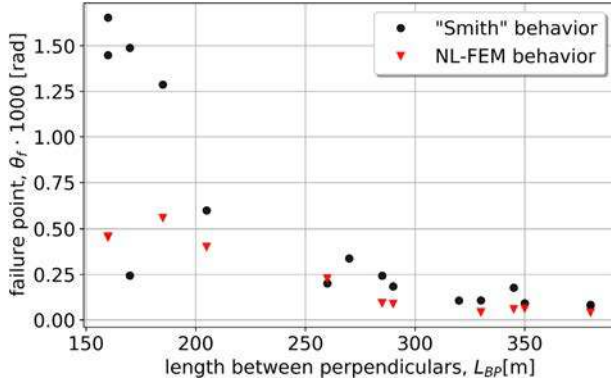


Fig. 10. Failure point vs. length between perpendiculars.

more, the structure collapses. Therefore, the focus is not on the post-collapse behavior, but only on the occurrence or not of the collapse. It is important to mention that the hull girder's collapse is reached when the relative plastic rotation angle becomes greater than the failure point, as shown in Fig. 4. Then, for the same scaled irregular wave train, the linear whipping response and the quasi-static response are also calculated for the sake of comparison with the nonlinear response.

The nonlinear whipping response is computed using the software DYANA2, developed by the authors for solving the fully-coupled hydro-elastoplastic problem as presented in Section 2. Within the calculation of the nonlinear whipping responses, the behavior of the nonlinear hinge can be either from the "Smith" method or from the "NL-FEM" method. Therefore, for the following numerical results, the difference between "Smith" behavior and "NL-FEM" behavior pertains to the characteristic behavior of the nonlinear hinge. It should be noted that currently, there is no data available, neither model- nor full-scale experiments, to validate the nonlinear whipping model. However, the structural part has been validated with analytic computations for the linear response, and the nonlinear response has been validated against the commercial NL-FEM software ABAQUS. Besides, the hydroelastic model has been validated by comparison with HOMER2, a hydro-structure interaction tool developed and maintained by Bureau Veritas (Derbanne et al., 2010). For the validations and verifications please refer to Jagite (2020).

Furthermore, the linear whipping response is calculated by assuming a linear-elastic structural behavior. This means that both the vertical displacement and the nodal rotations field are continuous at the nonlinear hinge's location. Aside from that, the quasi-static response under still water and wave-induced low-frequency loads is computed by disregarding the slamming loads.

As an illustration, Fig. 11 presents the nonlinear whipping response using the nonlinear behavior calculated by the simplified "Smith" approach, the linear whipping response, and the quasi-static one obtained for ship S04 considering the same irregular wave train. Thus, the following values are calculated:

- $M_{whip\ NL} = M_U$ representing the maximum nonlinear whipping response calculated as the internal bending moment obtained using the hydroelastoplastic model when the hull girder is subjected to nonlinear loads;
- $M_{whip\ Lin}$ representing the maximum linear whipping response calculated as the internal bending moment obtained on a linear dynamic structural model when the hull girder is subjected to nonlinear loads;
- M_{QS} representing the maximum quasi-static response calculated as the internal bending moment obtained when the hull girder is subjected to the usual "quasi-static" loads (still water + wave-induced low-frequency bending moment)).

Moreover, we define the dynamic ultimate capacity factor γ_{DU} as the ratio between the maximum linear whipping response $M_{whip\ Lin}$ and the maximum nonlinear whipping response $M_{whip\ NL}$. The dynamic ultimate capacity factor can be seen as the maximum allowable linear whipping response on a scenario where the nonlinear whipping response reaches the failure point, and it is calculated as follows:

$$\gamma_{DU} = \frac{M_{whip\ Lin}}{M_{whip\ NL}} \quad (12)$$

It is worth mentioning that in the investigation reported by Derbanne et al. (2016), a similar definition of the dynamic ultimate capacity factor is used. Thus, we can directly compare the values of γ_{DU} calculated by two different methods. Moreover, this dynamic ultimate capacity factor can be used in the verification of the hull girder ultimate strength by writing the design equation as follows:

$$M_{whip\ Lin} < \gamma_{DU} \cdot M_U \quad (13)$$

Going back to the literature, according to Veritas (2015), the design equation for the verification of the ultimate strength assessment including the effect of whipping can be written as follows:

$$M_{QS} + \gamma_{DU}^{(DNV)} (M_{whip\ Lin} - M_{QS}) < M_U \quad (14)$$

where $\gamma_{DU}^{(DNV)}$ is fixed to 0.9 and represents the factor reducing the effectiveness of whipping during collapse, which can be expressed as follows:

$$\gamma_{DU}^{(DNV)} = \frac{M_{whip\ NL} - M_{QS}}{M_{whip\ Lin} - M_{QS}} \quad (15)$$

4.1. Equivalent design wave

The nonlinear whipping response is firstly calculated by subjecting the hull girder to an EDW of type response conditioned wave (RCW) (Veritas, 2019a). A typical EDW of type RCW is defined as an irregular wave train containing several components, leading to the mean of all possible responses on a uni-directional sea-state. Hence, the analysis of the structural response is performed in a simple but realistic loading sequence, composed of a constant component given by the still-water bending moment, a low-frequency one given by the wave loading, and a high-frequency load component given by the response under impulsive loading (i.e., slamming). In the iterative algorithm employed for calculating the maximum nonlinear whipping response, the wave height is gradually scaled, and thus, the still-water component will remain constant while the dynamic components will increase nonlinearly. Once the maximum EDW height is obtained, the linear whipping response and the quasi-static response are calculated.

The corresponding linear and nonlinear responses obtained for ship S12 using the nonlinear behavior calculated by the NL-FEM approach are exhibited in Fig. 12. Around the instant $t = 0$, the internal bending moment reaches the yield limit, and the relative plastic rotation angle increases significantly, resulting in permanent plastic deformations. It should be noted that for the example shown in Fig. 12, the dynamic ultimate capacity factor γ_{DU} is equal to 1.0018. The nonlinear structural response reduces the whipping effectiveness, and thus, the nonlinear whipping response is below the linear one. The time variation of the relative plastic rotation angle between the aft- and the fore-beams is shown in Fig. 13(a), while Fig. 13(b) shows the capability of the presented model to follow the precomputed behavior describing the nonlinear relationship between the internal bending moment and the plastic rotation angle. As previously discussed, the nonlinear hinge model accounts for the permanent plastic deformation. Besides, the elastic part is considered fully linear, and the loading and the unloading path are identical even after the appearance of significant plastic deformations. The loading and the unloading of the elastic path are shown in Fig. 13(b) as vertical lines.

The above-mentioned procedure is repeated for all the ships presented in Table 1. It is important to mention that the hull girder is

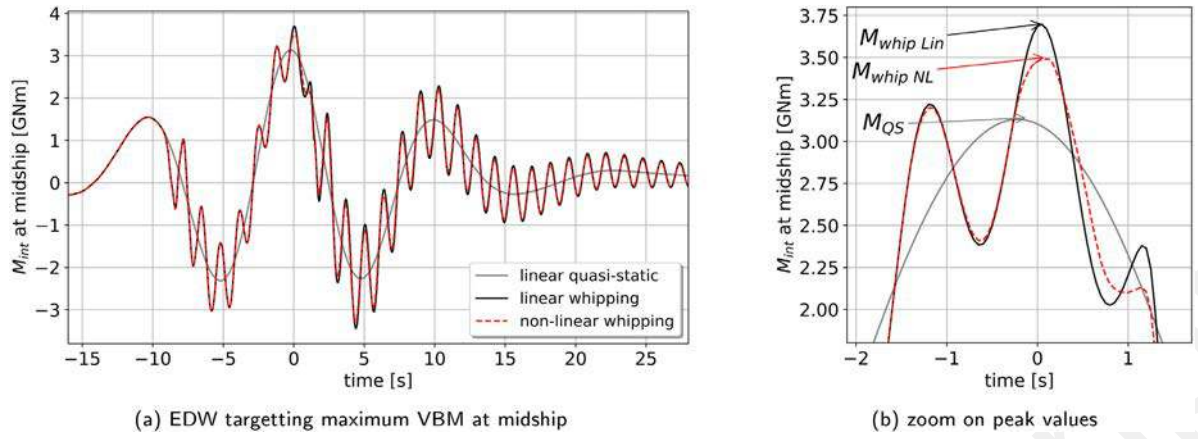


Fig. 11. Example of linear vs. nonlinear whipping for ship S04 under an equivalent design wave (EDW), using the nonlinear behavior computed by “Smith” approach.

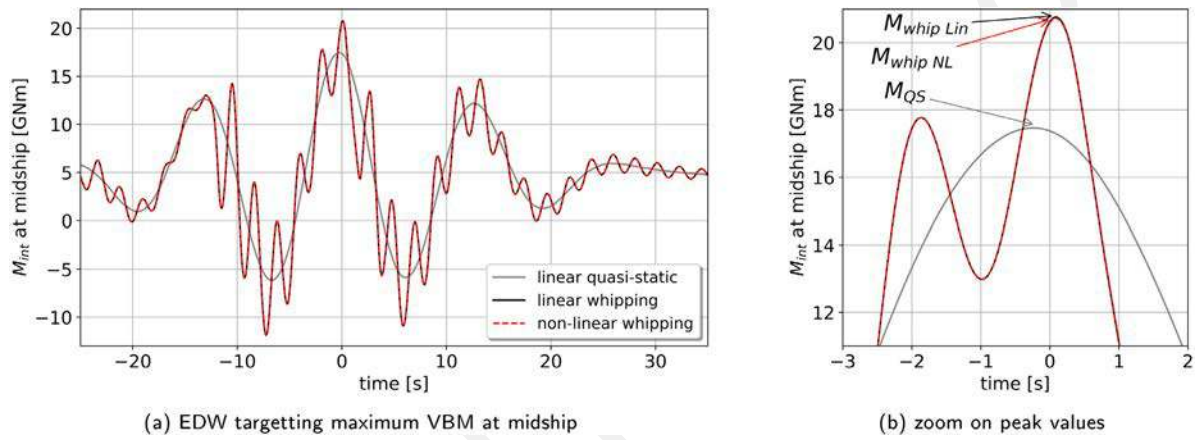


Fig. 12. Example of linear vs. nonlinear whipping for ship S12 under an EDW.

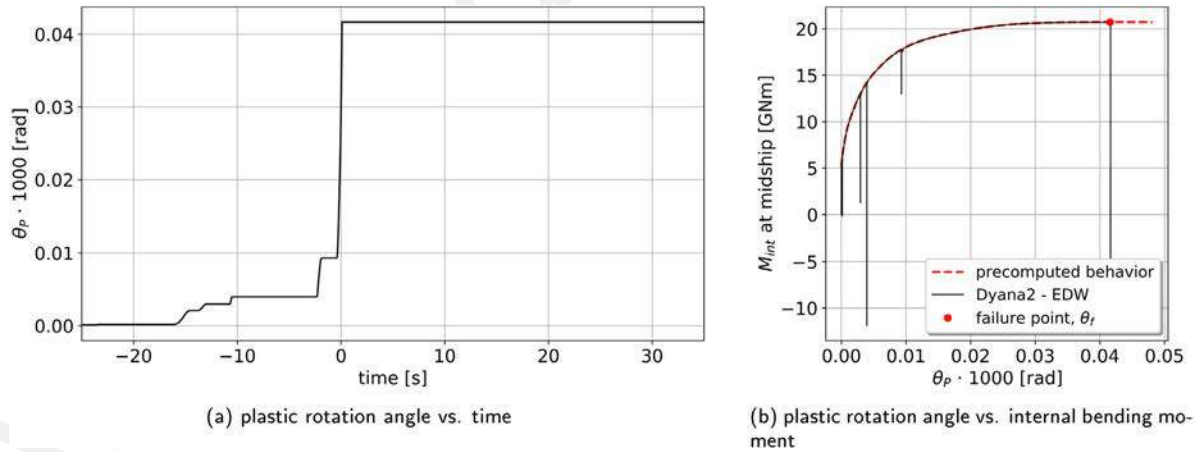


Fig. 13. Increase of the relative plastic rotation angle for ship S12 under an EDW of type RCW.

modeled with twelve elements for every ship, while for the hydrodynamic mesh, about 5000 panels are used. The structural damping is set to about 2% of the critical damping of the first two eigenmodes. The linear and nonlinear whipping responses are calculated for a forward speed of five knots, as recommended in Veritas (2019b). Moreover, the EDW-s of type RCW are created to maximize the hogging bending moment at midship using the so-called North Atlantic scatter diagram. The significant wave height H_s and the significant wave period T_p of the EDW for the considered ships are depicted in Table 2. The

fully coupled hydroelastoplastic calculations are performed using a fixed time step of 0.05 s. Convergence studies on different modeling parameters have been performed and can be found in Jagite (2020). Furthermore, it should be noted that when subjecting the hull-girder to an equivalent design wave, the computational time is only three seconds for each second in real-time. Thus, the developed methodology for solving the nonlinear hydroelastoplastic problem is efficient and allows for a fast evaluation of the nonlinear whipping response.

Table 2

Characteristics of the EDW of type RCW for the considered ships.

Ship	S01	S02	S03	S04	S05	S06	S07	S08	S09	S10	S11	S12	S13	S14
H_s [m]	10.5	10.6	10.7	10.5	10.7	10.7	11.0	11.6	11.5	11.0	12.0	12.1	12.2	12.3
T_p [s]	13.4	13.4	13.4	13.4	13.4	13.4	14.8	14.8	14.8	14.8	14.8	14.8	16.2	16.2

Table 3

Dynamic ultimate capacity factor of the considered container ships.

Ship	L_{BP} [m]	"Smith" behavior				NL-FEM behavior			
		$\theta_f \cdot 10^3$ [rad]	$\frac{M_{QS}}{M_U}$	γ_{DU}	$\gamma_{DU}^{(DNV)}$	$\theta_f \cdot 10^3$ [rad]	$\frac{M_{QS}}{M_U}$	γ_{DU}	$\gamma_{DU}^{(DNV)}$
S01	160	1.6544	0.7971	1.0722	0.7376	0.4575	0.7562	1.0234	0.9124
S02	160	1.4488	0.7609	1.0646	0.7874	0.4536	0.7260	1.0222	0.9249
S03	170	0.2430	0.7600	1.0112	0.9556	–	–	–	–
S04	170	1.4882	0.8969	1.0589	0.6362	–	–	–	–
S05	185	1.2872	0.9715	1.0381	0.4278	0.5597	0.9537	1.0196	0.7024
S06	205	0.6009	0.9052	1.0175	0.8440	0.4007	0.9066	1.0199	0.8245
S07	260	0.2006	0.9043	1.0071	0.9305	0.2275	0.9058	1.0094	0.9093
S08	270	0.3378	0.8012	1.0133	0.9375	–	–	–	–
S09	285	0.2429	0.8553	1.0128	0.9188	0.0919	0.8495	1.0052	0.9669
S10	290	0.1839	0.9386	1.0074	0.8930	0.0883	0.9348	1.0033	0.9513
S11	320	0.1061	0.8479	1.0043	0.9723	–	–	–	–
S12	330	0.1070	0.8453	1.0051	0.9679	0.0419	0.8429	1.0018	0.9884
S13	345	0.1771	0.8449	1.0096	0.9420	0.0590	0.8395	1.0031	0.9809
S14	350	0.0911	0.8463	1.0052	0.9670	0.0624	0.8441	1.0019	0.9880

At first, the nonlinear hinge behavior calculated using the simplified "Smith" method is used to calculate the nonlinear whipping response. Then, the more realistic nonlinear hinge behavior obtained from the NL-FEM method is used. It should be noted that the nonlinear behavior calculated using the NL-FEM method is available only for ten out of fourteen considered ships due to the high computational time required.

The dynamic ultimate capacity factors calculated with Eq. (12), and the whipping effectiveness coefficient calculated with Eq. (15) are summarized in Table 3, Fig. 14, and Fig. 15.

From Fig. 14(a), it can be observed that the dynamic ultimate capacity factors obtained using the nonlinear behavior computed using the "Smith" approach are significantly higher than the ones obtained using the nonlinear behavior computed using the more advanced NL-FEM analyses. This is expected since the failure points computed by the NL-FEM analyses are below the ones obtained by the simplified "Smith" approach, as depicted in Fig. 10. The dynamic ultimate capacity factor is highly dependent on the failure point, and it decreases with the decrease of the failure point, as shown in Fig. 14(b). Moreover, it can be observed that there is a linear dependency between the dynamic ultimate capacity factor and the failure point. This linear dependency can be associated with the ratio between the kinetic energy given by the external forces and the energy dissipated to follow the precomputed behavior through plastic deformations.

More importantly we can observe that the dynamic ultimate capacity factor is always greater than unity. This basically means that the nonlinear whipping response calculated using the fully-coupled hydroelastoplastic method is always smaller than the linear whipping response. For ultra-large container ships above 250 m, the dynamic ultimate capacity factor is under 1.01, when the nonlinear behavior computed by NL-FEM approach is used, or up to 1.015, when the nonlinear behavior calculated by the simplified "Smith" approach is used, as Fig. 14(a) bears out. However, for smaller ships, the dynamic ultimate capacity factor can be up to 1.025 when the nonlinear behavior computed by the NL-FEM method is used or up to 1.07 when the nonlinear behavior calculated by the simplified "Smith" approach is used. The results obtained on smaller ships are raising some questions regarding the capability of the simplified "Smith" approach for the calculation of the elastoplastic behavior, which is used to derive the nonlinear behavior of the hinge.

Furthermore, the whipping effectiveness is calculated using Eq. (15), and exhibited in Fig. 15. On the one hand, it can be observed that for container ships above 250 m, the whipping effectiveness is above 0.9 and increases when the ship length is increasing. On the other hand, for the ships under 250 m, there is a significant difference in the results when different methods are used to define the nonlinear behavior curves. More importantly, it can be seen that the whipping effectiveness value recommended by Veritas (2015) is not conservative. Besides, the values obtained for all ULCS are above the fixed value of 0.9. It is further important to point out that when calculating the whipping effectiveness, its value is highly dependent on the ratio between the quasi-static response and the nonlinear whipping response. If the ratio M_{QS}/M_U is close to unity, then the dynamic components will be very small. Thus, the ratio between the nonlinear whipping contribution to the linear whipping contribution might lead to smaller values of the whipping effectiveness, as it can be seen in Fig. 15(a) for ship S05 ($L_{BP} = 185$ meters).

In addition, the influence of the high-frequency response over the dynamic ultimate capacity factor is investigated. This aspect was previously analyzed by Derbanne et al. (2016), showing that when the ratio between the usual quasi-static bending moment M_{QS} and the nonlinear whipping response $M_{whip\ NL}$ increases the dynamic ultimate capacity factor decreases. In their paper, the sum of still-water and wave excitation was varied from 0.8 to 0.98 of the ultimate strength. A similar approach is employed in this research work, by adjusting the intensity of the slamming load, different ratios between the whipping response and the "usual" quasi-static response can be obtained. It is worth mentioning that the same equivalent design waves are used for each ship; however, these waves are to be scaled with different factors until the maximum wave height that can be sustained without collapsing is obtained. The numerical results are presented in Fig. 16(a) when the nonlinear behavior computed using the simplified "Smith" method is used, and in Fig. 16(b) when the nonlinear behavior calculated by NL-FEM analysis is used.

The results presented in Figs. 16(a) and 16(b) confirm the dependency between the quasi-static ratio and the dynamic ultimate capacity factors. Moreover, it can be seen that when the ratio between the "quasi-static" response and the nonlinear whipping response gets closer to unity, the dynamic ultimate capacity factor decreases toward one.

As previously pointed out, it is observed that the whipping effectiveness, noted as $\gamma_{DU}^{(DNV)}$, may reach some very small values when the ratio between the "quasi-static" response and the nonlinear whipping response gets closer to unity. Therefore, the variation of whipping effectiveness calculated for different M_{QS}/M_U ratios is presented in Fig. 17, illustrating the above mentioned behavior. Please note that for ULCS above 250 m, when the M_{QS}/M_U ratio varies from 0.8 to 0.95, the whipping effectiveness varies between 0.96 and 0.99 when the nonlinear behavior computed by NL-FEM approach is used, and between 0.86 and 0.97 when the nonlinear behavior computed by "Smith" approach is used.

4.2. Design sea state

The most realistic loading sequence that one could use when designing of modern ships is a design sea-state (DSS). Thus, instead of using a single equivalent design wave that maximizes the vertical bending moment at midship, a longer irregular sea-state is considered. When the ship encounters a significant wave, the relative plastic rotation angle will increase, and thus, after several significant waves, the plastic deformation will accumulate. Therefore, the focus of the current investigation is to see how the memory effect due to the cumulative permanent plastic deformation affects the nonlinear whipping response. However, since the computational cost increases significantly when a design sea-state is used instead of an equivalent design wave, only some ships will be considered for computing the nonlinear whipping responses.

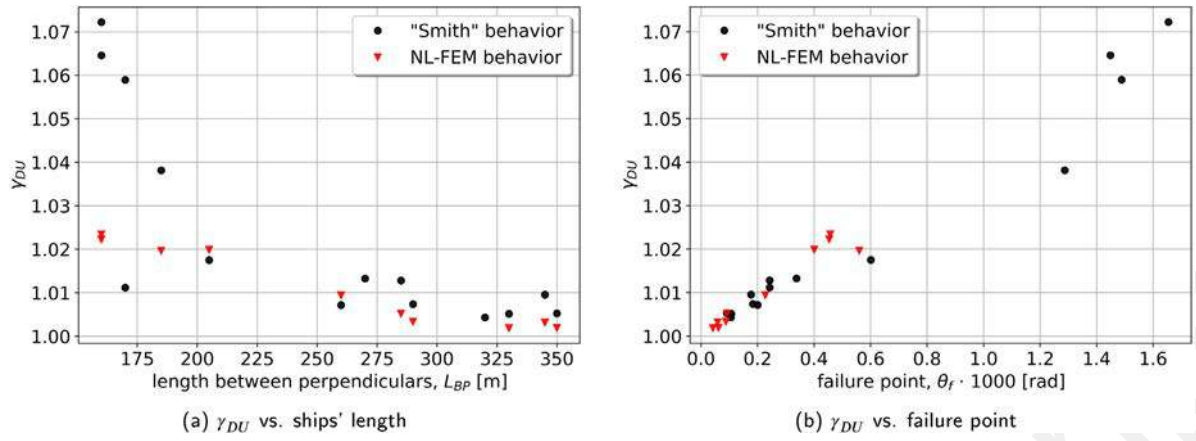


Fig. 14. Dynamic ultimate capacity factor of the considered container ships.

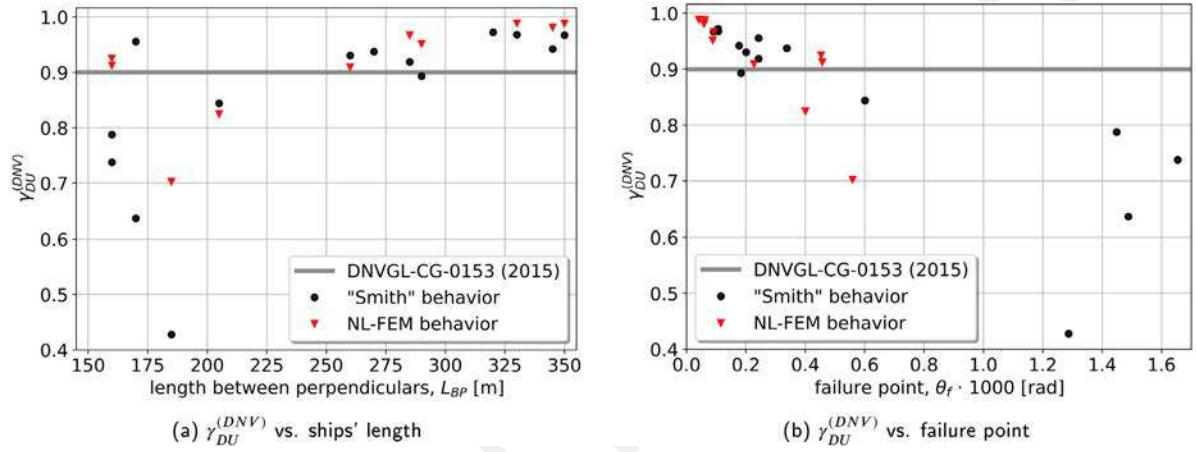


Fig. 15. Whipping effectiveness coefficient of fourteen container ships.

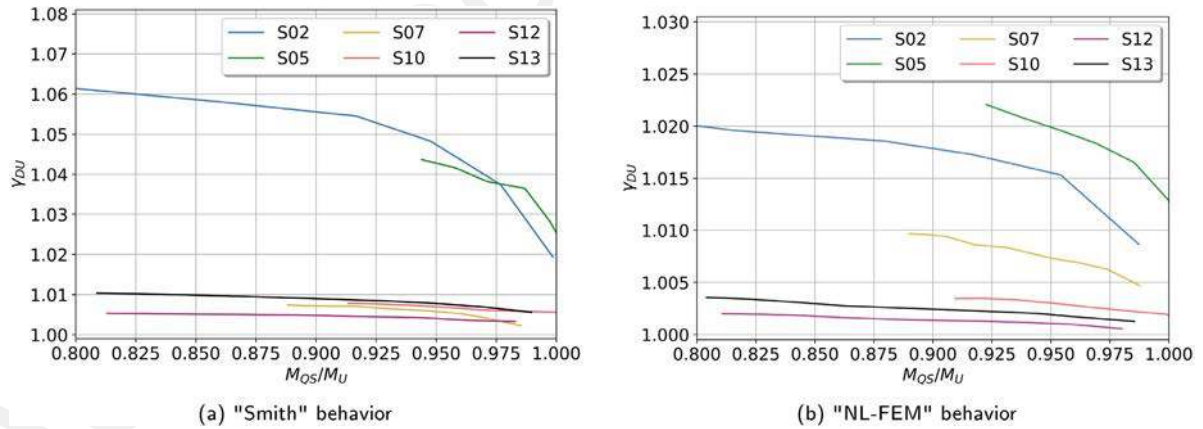


Fig. 16. Dynamic ultimate capacity factor vs. M_{QS}/M_U coefficient.

The first ship chosen is ship S12, with a length between perpendiculars of 330 m, and cargo-carrying capacity of 9300 TEU. The design sea state is defined using the JONSWAP spectrum with a significant wave height of $H_s=16.8$ meters and a significant wave period of $T_p=16.2$ s. It can be seen that three significant waves are encountered at the instant $t=750$, $t=1300$, and $t=3400$ s, respectively. Using the hydroelastoplastic model, the amplitude of the design sea state is gradually scaled until the nonlinear whipping response becomes equal to the ultimate strength, i.e., $M_{whip\ NL} = M_U$. Then, the linear whipping response, and

the quasi-static response are calculated for the same maximum design sea state. The linear and nonlinear whipping responses obtained using the nonlinear behavior calculated with NL-FEM approach, are shown in Fig. 18.

The evolution of the relative plastic rotation angle is shown in Fig. 19(a). It can be observed that at the instant $t=750$ s when the ship encounters the first significant wave, the plastic rotation angle increases. Then the plastic rotation angle is maintained until $t = 1400$ when a second significant wave is encountered, and the relative plastic

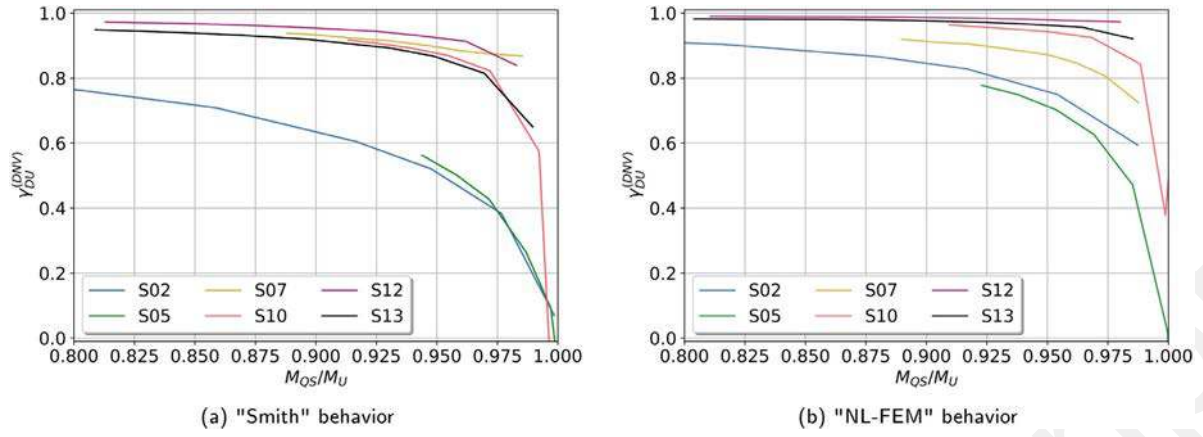


Fig. 17. Whipping effectiveness vs. M_{QS}/M_U coefficient.

Table 4

Dynamic ultimate capacity factors and whipping effectiveness under design sea state.

Case		S02	S05	S10	S12	S13
"Smith" behavior	M_{QS}/M_U	DSS	0.7326	0.7848	0.8885	0.8541
		EDW	0.7609	0.9715	0.9386	0.8453
	γ_{DU}	DSS	1.0294	1.0097	1.0053	1.0050
		EDW	1.0646	1.0381	1.0074	1.0096
	$\gamma_{DU}^{(DNV)}$	DSS	0.9009	0.9569	0.9544	0.9669
		EDW	0.7874	0.4278	0.8930	0.9420
NL-FEM behavior	M_{QS}/M_U	DSS	0.7206	0.7766	0.8855	0.8512
		EDW	0.7260	0.9537	0.9348	0.8429
	γ_{DU}	DSS	1.0122	1.0075	1.0016	1.0015
		EDW	1.0222	1.0196	1.0033	1.0018
	$\gamma_{DU}^{(DNV)}$	DSS	0.9582	0.9673	0.9859	0.9903
		EDW	0.9249	0.7024	0.9513	0.9809

rotation angle is further increased. Finally, at $t=3400$ s, the plastic rotation angle almost reaches the failure point. If the amplitude of the design sea state is increased a little bit more, the failure point will be reached, and the structure will collapse. Moreover, the hardening behavior and the accumulation of plastic deformations can be seen in Fig. 19(b).

Using the same design sea state, the nonlinear whipping response is computed using the nonlinear behavior calculated by the simplified "Smith" approach. On the one hand, when using the nonlinear behavior computed by the NL-FEM approach, the dynamic ultimate capacity factor is 1.0015. On the other hand, when using the nonlinear behavior computed by the simplified "Smith" approach, the maximum value obtained is 1.0050. Thus, the values obtained on a design sea state are smaller than those obtained on an equivalent design wave: 1.0018 and 1.0051, respectively. This aspect was also pointed out by Derbanne et al. (2016), showing that the dynamic ultimate capacity factor decreases when more realistic loading sequences are used.

In addition, the calculation of the nonlinear whipping response under the design sea state is performed for ships S02, S05, S10, and S13. The dynamic ultimate capacity factor and the whipping effectiveness are summarized in Table 4. It can be observed that for all considered ships, both the dynamic ultimate capacity factors and the whipping effectiveness obtained on design sea-state are smaller than the ones obtained on equivalent design waves.

4.3. Results discussion

The numerical results obtained using the newly developed hydroelastoplastic model are further compared with the ones obtained by Derbanne et al. (2016). It is important to point out that in Derbanne et al. (2016) the investigations of the dynamic ultimate strength are

Table 5

Dynamic ultimate capacity factor from Derbanne et al. (2016).

Method	$* \frac{M_{QS}}{M_U}$	Ship 2, $\bar{\chi}_f = 1.39$		Ship 13, $\bar{\chi}_f = 1.23$	
		$L_{BP} = 280$ [m]		$L_{BP} = 375$ [m]	
		γ_{DU}	$\gamma_{DU}^{(DNV)}$	γ_{DU}	$\gamma_{DU}^{(DNV)}$
Energy conservation (Eq. (15))	0.8	1.33	0.38	1.21	0.49
Energy conservation (Eq. (14))	0.8	1.29	0.41	1.17	0.54
Equivalent design wave	0.8	1.25	0.44	1.15	0.57
Design sea state	0.8	1.11	0.65	1.08	0.71

performed only on ULCS, ranging from 264 to 378 m. For these ships, the failure point's location, calculated as the non-dimensionalized curvature, ranges from 1.23 to 1.39. These values are very similar to the ones obtained on the ULCS considered in the present research work, as shown in Fig. 5(b).

In the study reported by Derbanne et al. (2016), the dynamic ultimate strength is calculated using a single DOF system, which can be expressed as:

$$\frac{1}{\omega_0^2} \ddot{\chi}(t) + \frac{2\eta}{\omega_0} \dot{\chi}(t) + f(\chi(t)) = F(t) \quad (16)$$

where $F(t)$ represents the excitation term. χ represents the curvature, and $f(t)$ represents the internal bending moment. It should be mentioned that the nonlinear behavior of each ship, represented by the relationship between the curvature and the internal bending moment, was calculated using the simplified "Smith" approach. More importantly, by using a single DOF system, the nonlinear curvature is uniformly distributed along the ship's length. This represents a big limitation of the structural model presented in Eq. (16) since, in reality, the collapse of the hull girder is very localized.

Using the model presented in Eq. (16), Derbanne et al. (2016) firstly calculated the dynamic ultimate capacity factor for a simple, but unrealistic, loading sequence composed of pure slamming impact on calm water by using the energy conservation. Besides, the dynamic ultimate capacity factor was calculated for more realistic loading sequences as an equivalent design wave or design sea state. The results obtained by Derbanne et al. (2016) for the ships with the lowest and the highest failure point, which are also the ones with the lowest and the highest dynamic ultimate capacity factor, are summarized in Table 5.

The dynamic ultimate capacity factors from Derbanne et al. (2016) (Table 5), and the ones obtained in the present research work (see Tables 3 and 4) are compared in Fig. 20.

One of the conclusions from Derbanne et al. (2016) was that too simple excitation sequences, such as a pure slamming impact on calm water, are overestimating the dynamic ultimate capacity factor. This aspect is clearly visible in Fig. 20. Moreover, it can be observed that

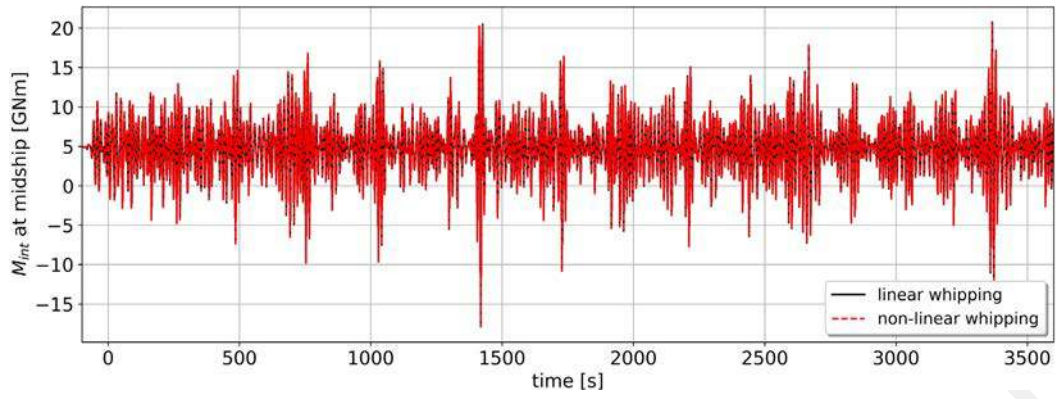


Fig. 18. Resulting time series for ship S12, using the nonlinear behavior calculated by NL-FEM approach.

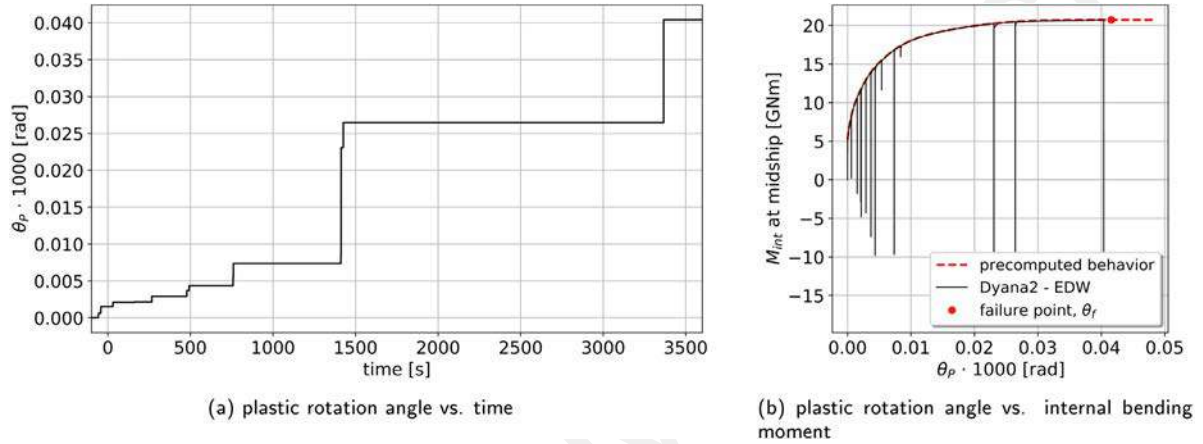


Fig. 19. Increase of the relative plastic rotation angle on a design sea state for ship S12.

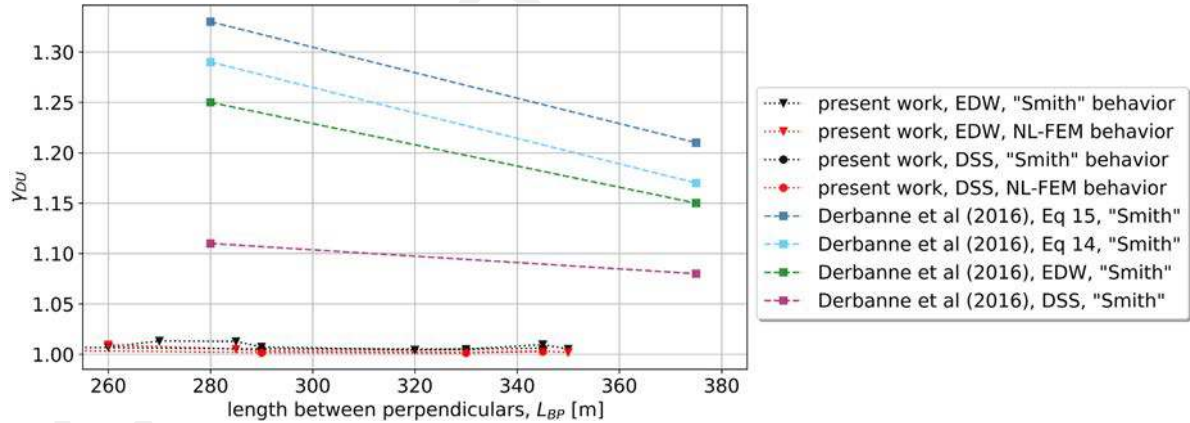


Fig. 20. Comparison of dynamic ultimate capacity factors.

when the nonlinear whipping response is calculated on a design sea state, instead of an equivalent design wave, the dynamic ultimate capacity factors are reduced.

More importantly, the numerical results depicted in Fig. 20 are showing that there is a significant reduction of the dynamic ultimate capacity factor calculated by two different methods. On the one hand, in the newly developed hydroelastoplastic method, the plastic deformations are very localized along the hull girder, i.e., reduced at a node of the FE model. On the other hand, in the investigation reported by Derbanne et al. (2016) the plastic deformations are considered uniformly distributed along the hull girder. Therefore, it can be said

that it is essential to use a realistic structural model instead of a single degree of freedom model.

5. Conclusions

The paper firstly presents a new approach developed to compute the nonlinear whipping response using a fully coupled hydroelastoplastic model. Within the proposed method, the structure is modeled as two non-uniform Timoshenko beams connected via a nonlinear hinge, while the hydrodynamic part is modeled using the 3D boundary element method. The exact coupling between the structural model and the

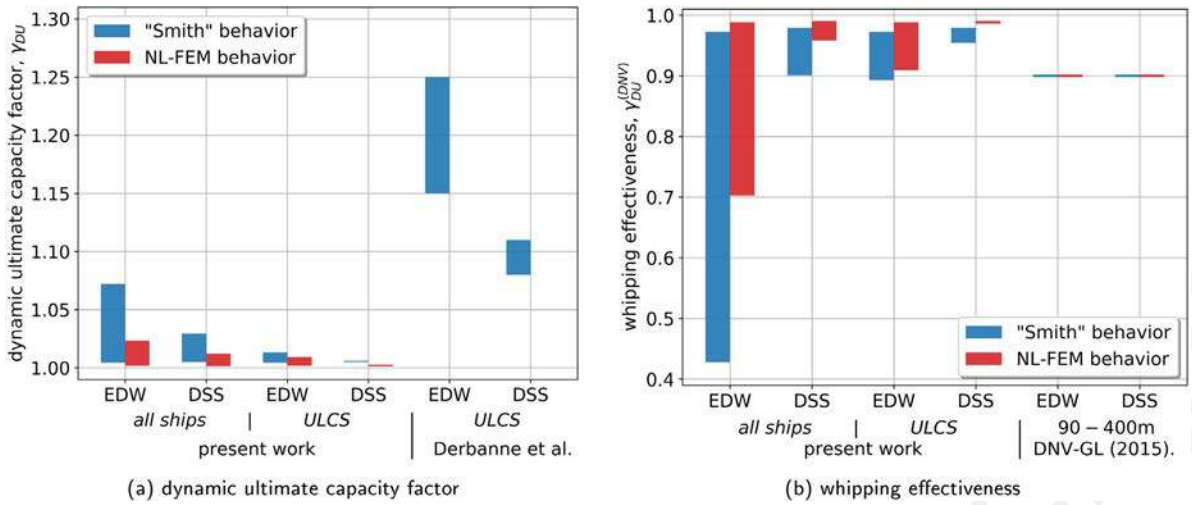


Fig. 21. Summary of the dynamic ultimate capacity factor and whipping effectiveness coefficient.

hydrodynamic one is achieved by constructing the hydrodynamic BVP-s for each shape function of the finite elements. After solving the complex BVP-s for a range of frequencies, the hydrodynamic coefficients in terms of added mass, wave damping, and wave excitation are determined. The time-domain simulation is then performed by making use of the frequency-dependent hydrodynamic coefficients to calculate the diffracted-incident wave loads. In addition, the radiation force is calculated from the memory-response functions and the past history of the velocities. The nonlinear pressures resulting from slamming are calculated on multiple 2D sections and later integrated over the 3D hydrodynamic mesh. Finally, the hydroelastoplastic problem is solved in the time-domain using numerical integration, where different iterations are used to handle the nonlinearities. The hydroelastoplastic model allows for a fast computation of the nonlinear whipping response (i.e., considering the nonlinear structural behavior) on realistic scenarios such as equivalent design waves or design sea states. Comparing to a strongly coupled CFD-FEM approach, where both domains should be considered nonlinear, the proposed approach's computational time is significantly reduced: from days to minutes.

Secondly, this paper presents the numerical investigation of the nonlinear whipping response on a database of fourteen container ships ranging from 160 m to 350 m. The nonlinear hinge's behavior is described by the nonlinear relationship between the internal bending moment and the relative plastic rotation angle, which is derived from the well-known moment-curvature curve used to describe the ultimate strength of a ship section. For the considered ships, the nonlinear behavior is calculated using two different methods:

- (i) the simplified "Smith" approach where the nonlinear curvature is associated with the entire length between two reinforced frames;
- (ii) the NL-FEM approach where the plastic area is very localized between two web frames.

When comparing the output of the two methods, it is observed that the failure point, defined as the relative plastic rotation angle at the moment when the internal bending moment is equal to the ultimate strength, is significantly lower in the results obtained from the more advanced approach based on NL-FEM. This aspect raises some questions regarding the usability of the simplified "Smith" approach in computing the nonlinear behavior curves accurately.

Two coefficients, noted γ_{DU} and $\gamma_{DU}^{(DNV)}$, are derived in order to account for the influence of the nonlinear structural behavior over the whipping response. The numerical results show that both coefficients

are highly dependent on the ratio between the quasi-static response to the total nonlinear whipping response, and on the failure point.

The dynamic ultimate capacity factor calculated on equivalent design waves varies from 1.005 to 1.072 when the nonlinear behavior from the simplified "Smith" approach is used, and from 1.001 to 1.023 when the nonlinear behavior calculated by the NL-FEM approach is used. It should be mentioned that for ULCS (above 250 m), the dynamic ultimate capacity factor calculated varies from 1.005 to 1.013 when the nonlinear behavior from the simplified "Smith" approach is used, and from 1.001 to 1.010 when the nonlinear behavior calculated by the NL-FEM approach is used.

The whipping effectiveness calculated on equivalent design waves varies from 0.42 to 0.97 when the nonlinear behavior calculated by the simplified "Smith" approach is used, and from 0.70 to 0.99 when the nonlinear behavior calculated by the NL-FEM approach is used. Moreover, for ULCS, the whipping effectiveness varies from 0.89 to 0.97 when the nonlinear behavior calculated by the simplified "Smith" approach is used, and from 0.90 to 0.99 when the nonlinear behavior calculated by the NL-FEM approach is used. Therefore, it seems that the value $\gamma_{DU}^{(DNV)} = 0.9$ introduced by Veritas (2015) is not conservative.

In addition, when the nonlinear whipping response is calculated on a design sea state, the dynamic ultimate capacity factor decreases, while the whipping effectiveness increases. This aspect was also pointed out by Derbanne et al. (2016). Thus, it can be said that it is of paramount importance to use realistic loading sequences when analyzing the influence of nonlinear structural behavior over the slamming-induced whipping response.

Moreover, it was shown the importance of using a realistic structural model. The dynamic ultimate capacity factors obtained using the single DOF structural model proposed by Derbanne et al. (2016) are significantly bigger than the ones obtained from the newly developed method. This difference can be explained by the fact that in the single DOF model, the plasticity is uniformly distributed along the hull girder, while in the nonlinear hinge model, the plasticity occurs only within one frame.

Finally, the above mentioned numerical results are summarized in Fig. 21. The outcome of this study provides useful information regarding the effects of nonlinear structural behavior on the slamming-induced whipping response of ships. For ultra-large container ships, the dynamic ultimate capacity factor defined as the ratio between the linear whipping response and the nonlinear whipping response varies from 1.001 to 1.013. Therefore, it can be concluded that the nonlinear structural behavior can be neglected in the analysis of the maximum hydroelastic response. Moreover, the effectiveness of whipping varies

from 0.89 to 0.99 which firstly shows that the fixed value of 0.9 recommended by Veritas (2015) is not conservative. Thus, the effectiveness of whipping should no be reduced.

CRedit authorship contribution statement

George Jagite: Conceptualization, Methodology, Software, Validation, Investigation, Formal analysis, Visualization, Writing – original draft, Review & editing. **Quentin Derbanne:** Conceptualization, Resources, Visualization, Supervision. **Sime Malenica:** Conceptualization, Methodology, Writing – review. **Fabien Bigot:** Conceptualization, Methodology, Writing – review. **Herve Le Sourn:** Supervision, Resources, Writing – review. **Patrice Cartraud:** Supervision, Resources, Writing – review.

Declaration of competing interest

The authors declare that they have no known competing financial interests or personal relationships that could have appeared to influence the work reported in this paper.

Acknowledgments

The present research work was undertaken at Ecole Centrale de Nantes, France, as a part of a Ph.D. thesis on the analysis of whipping effects over the hull girder's ultimate strength. The first author is pleased to acknowledge the funding and support of Bureau Veritas via BV-ECN cooperation.

References

ABAQUS, 2017. Dassault systemes simulia corp, johnston, RI, USA.
 Bishop, R.E., Price, W.G., 1979. Hydroelasticity of Ships. Cambridge University Press.
 Branch, M.A.I., 2008. Report on the Investigation of the Structural Failure of MSC Napoli, English Channel on 18 January 2007. Technical Report, Marine Accident Investigation Branch.
 Chen, X.-j., Wu, Y.-s., Cui, W.-c., Jensen, J.J., 2006. Review of hydroelasticity theories for global response of marine structures. *Ocean Eng.* 33 (3–4), 439–457.
 ClassNK, 2014. Investigation Report on Structural Safety of Large Container Ships. Technical Report, ClassNK.
 Cummins, W., 1962. The Impulse Response Function and Ship Motions. Technical Report, David Taylor Model Basin Washington DC.
 De Lauzon, J., Grgic, M., Derbanne, Q., Malenica, S., 2015. Improved generalized Wagner model for slamming. In: *Proceedings of 7th International Conference on Hydroelasticity in Marine Technology*, Split, Croatia, pp. 561–574.
 Derbanne, Q., de Lauzon, J., Bigot, F., Malenica, S., 2016. Investigations of the dynamic ultimate strength of a ship's hull girder during whipping. In: *Proceedings of PRADS2016*, vol. 4, 8th.
 Derbanne, Q., Malenica, S., Tuitman, J., Bigot, F., Chen, X., 2010. Validation of the global hydroelastic model for springing & whipping of ships. In: *11th International Symposium on Practical Design of Ships and Other Floating Structures*, Rio de Janeiro, pp. 331–340.
 Dow, R., 1981. Evaluation of ultimate ship hull strength. In: *Proc. Symp. on Extreme Loads Response*, pp. 133–148.
 Ergin, A., Alley, E., Brandt, A., Drummen, I., Hermundstad, O.A., Huh, Y.-C., Ivaldi, A., Liu, J., Malenica, S., el Moctar, B.O., et al., 2018. ISSC Committee II. 2–dynamic response. In: *Proceedings of the 20th International Ship and Offshore Structures Congress (ISSC 2018)*. IOS Press.
 Hilber, H.M., Hughes, T.J., Taylor, R.L., 1977. Improved numerical dissipation for time integration algorithms in structural dynamics. *Earthq. Eng. Struct. Dyn.* 5 (3), 283–292.
 Hirdaris, S., Temarel, P., 2009. Hydroelasticity of ships: recent advances and future trends. *Proc. Inst. Mech. Eng. M* 223 (3), 305–330.
 Iida, T., Umazume, K., 2020. Wave response of segmented floating plate and validation of its homogenized solution. *Appl. Ocean Res.* 97, 102083.
 Iijima, K., Fujikubo, M., 2012. Post-ultimate strength behavior of very large floating structure subjected to extreme wave loads. In: *ASME 2012 31st International Conference on Ocean, Offshore and Arctic Engineering*. American Society of Mechanical Engineers Digital Collection, pp. 109–116.
 Iijima, K., Fujikubo, M., 2015. Cumulative collapse of a ship hull girder under a series of extreme wave loads. *J. Mar. Sci. Technol.* 20 (3), 530–541.
 Iijima, K., Fujikubo, M., 2018. Hydro-elastoplastic behaviour of VLFS under extreme vertical bending moment by segmented beam approach. *Mar. Struct.* 57, 1–17.

Iijima, K., Kimura, K., Xu, W., Fujikubo, M., 2011. Hydroelasto-plasticity approach to predicting the post-ultimate strength behavior of a ship's hull girder in waves. *J. Mar. Sci. Technol.* 16 (4), 379–389.
 Jagite, G., 2020. Analysis of Slamming Induced Whipping Effects over the Ultimate Strength of Ships (Ph.D. thesis). École centrale de Nantes.
 Jagite, G., Bigot, F., Derbanne, Q., Malenica, S., Le Sourn, H., Cartraud, P., 2020a. Dynamic ultimate strength of a container ship under sagging condition. In: *ASME 2020 39th International Conference on Ocean, Offshore and Arctic Engineering*. American Society of Mechanical Engineers.
 Jagite, G., Bigot, F., Derbanne, Q., Malenica, S., Le Sourn, H., de Lauzon, J., Cartraud, P., 2019a. Numerical investigation on dynamic ultimate strength of stiffened panels considering real loading scenarios. *Ships Offshore Struct.* 1–13. <http://dx.doi.org/10.1080/17445302.2019.1601329>.
 Jagite, G., Bigot, F., Derbanne, Q., Malenica, S., Le Sourn, H., de Lauzon, J., Cartraud, P., 2020b. A parametric study on the dynamic ultimate strength of a stiffened panel subjected to wave- and whipping-induced stresses. *Ships Offshore Struct.* 1–15. <http://dx.doi.org/10.1080/17445302.2020.1790985>.
 Jagite, G., Le Sourn, H., Cartraud, P., Bigot, F., Derbanne, Q., Malenica, S., 2019b. Examination of the dynamic effects on the hull girder ultimate strength of ultra large container ships. In: *Trends in the Analysis and Design of Marine Structures: Proceedings of the 7th International Conference on Marine Structures (MARSTRUCT 2019)*, Dubrovnik, Croatia, 6–8 May 2019). CRC Press, pp. 137–149.
 Jagite, G., Malenica, S., Bigot, F., de Lauzon, J., Derbanne, Q., Le Sourn, H., Cartraud, P., 2020c. A new approach to compute the non-linear whipping response using hydro-elastoplastic coupling. In: *ASME 2020 39th International Conference on Ocean, Offshore and Arctic Engineering*. American Society of Mechanical Engineers.
 Kim, K.-H., Bang, J.-S., Kim, J.-H., Kim, Y., Kim, S.-J., Kim, Y., 2013. Fully coupled BEM-FEM analysis for ship hydroelasticity in waves. *Mar. Struct.* 33, 71–99.
 Kim, J.-H., Kim, Y., Korobkin, A., 2014. Comparison of fully coupled hydroelastic computation and segmented model test results for slamming and whipping loads. *Int. J. Naval Archit. Ocean Eng.* 6 (4), 1064–1081.
 Korobkin, A., 2004. Analytical models of water impact. *European J. Appl. Math.* 15 (6), 821.
 Korobkin, A., Malenica, S., 2005. Modified Logvinovich model for hydrodynamic loads on asymmetric contours entering water. In: *Proceedings of the 20th International Workshop on Water Waves and Floating Bodies*, Oslo, Norway.
 Lakshminarayana, P., Temarel, P., 2018. Fully coupled CFD/FEA investigations to predict the wave loads on a flexible containership.
 Malenica, S., 1998. Hydroelastic coupling of beam structural model with 3D hydrodynamic model. In: *2nd Int. Conf. on Hydroelasticity*.
 Matsumoto, T., Shigemi, T., Kidogawa, M., Ishibashi, K., Sugimoto, K., 2016. Examination of effect of lateral loads on the hull girder ultimate strength of large container ships. In: *ASME 2016 35th International Conference on Ocean, Offshore and Arctic Engineering*. American Society of Mechanical Engineers.
 Newmark, N.M., et al., 1959. A method of computation for structural dynamics. *J. Eng. Mech. Div.* 85 (3), 67–94.
 Oberhagemann, J., Shigunov, V., Radon, M., Mumm, H., Won, S.-I., 2015. Hydrodynamic load analysis and ultimate strength check of an 18000 TEU containership. In: *Proceedings of the 7th International Conference on Hydroelasticity in Marine Technology*, Split.
 Paik, J.K., 2018. *Ultimate Limit State Design of Steel-Plated Structures*, second ed. John Wiley & Sons.
 Paik, J.K., Kim, B.J., Seo, J.K., 2008. Methods for ultimate limit state assessment of ships and ship-shaped offshore structures: Part III hull girders. *Ocean Eng.* 35 (2), 281–286.
 Seng, S., 2012. *Slamming and Whipping Analysis of Ships* (Ph.D. thesis). DTU Mechanical Engineering.
 Seng, S., Benhamou, A., Monroy, C., Malenica, S., 2018. Hydroelastic simulations in OpenFOAM®: An efficient numerical implementation of the modal equations. *Hydroelast. Mar. Technol.*.
 Seng, S., Jensen, J.R., Malenica, S., 2014. Global hydroelastic model for springing and whipping based on a free-surface CFD code (openfoam). *Int. J. Naval Archit. Ocean Eng.* 6 (4), 1024–1040.
 Smith, C.S., 1977. Influence of local compressive failure on ultimate longitudinal strength of a ship's hull. In: *Proc. Int. Sym. on Practical Design in Shipbuilding*, pp. 73–79.
 Takami, T., Iijima, K., 2019. Numerical investigation into combined global and local hydroelastic response in a large container ship based on two-way coupled CFD and FEA. *J. Mar. Sci. Technol.* 1–17.
 Temarel, P., Bai, W., Bruns, A., Derbanne, Q., Dessi, D., Dhavalikar, S., Fonseca, N., Fukasawa, T., Gu, X., Nestegård, A., et al., 2016. Prediction of wave-induced loads on ships: Progress and challenges. *Ocean Eng.* 119, 274–308.
 Tuitman, J., Malenica, S., 2009. Fully coupled seakeeping, slamming, and whipping calculations. *Proc. Inst. Mech. Eng. M* 223 (3), 439–456.
 Ueda, Y., Rashed, S., 1984. The idealized structural unit method and its application to deep girder structures. *Comput. Struct.* 18 (2).
 Veritas, D.N., 2015. CG-0153 Fatigue and Ultimate Strength Assessment of Container Ships Including Whipping and Springing. Det Norske Veritas.
 Veritas, B., 2019a. Guidance for Long-Term Hydro-Structure Calculations. Bureau Veritas,

- Veritas, B., 2019b. Structural Rules for Container Ships. Bureau Veritas.
- Veritas, B., 2019c. MARS 2000 - 2D ship structural assessment software. User's Guide.
- Wagner, H., 1932. Über stoß-und gleitvorgänge an der oberfläche von flüssigkeiten. ZAMM 12 (4), 193–215.
- Weller, H.G., Tabor, G., Jasak, H., Fureby, C., 1998. A tensorial approach to computational continuum mechanics using object-oriented techniques. Comput. Phys. 12 (6), 620–631.
- Xu, W., Iijima, K., Fujikubo, M., 2011. Investigation into post-ultimate strength behavior of ship's hull girder in waves by analytical solution. In: ASME 2011 30th International Conference on Ocean, Offshore and Arctic Engineering. American Society of Mechanical Engineers Digital Collection, pp. 455–462.
- Yamada, Y., 2019. Approach to simulate dynamic elasto-plastic whipping response of global hull girder of a large container ship due to slamming load. In: The 29th International Ocean and Polar Engineering Conference. International Society of Offshore and Polar Engineers.
- Yoon, J.-S., Lee, P.-S., 2017. Towards hydro-elastoplastic analysis of floating plate structures. J. Fluids Struct. 71, 164–182.